UNITED NATIONS UNIVERSITY
UNU-GTP
Geothermal Training Programme

Orkustofnun, Grensasvegur 9,
IS-108 Reykjavik, Iceland

Reports 2014
Number 7

NATURAL-STATE MODEL UPDATE OF OLKARIA DOMES GEOTHERMAL FIELD

Maureen Nechesa Ambunya
Kenya Electricity Generating Company – KenGen
P.O. Box 785 – 20117
Naivasha
KENYA
mambunya@kengen.co.ke

ABSTRACT

The Olkaria Domes geothermal field is located at the southeast edge of the Greater Olkaria geothermal area (GOGA). The area is bound approximately by the Ol'Njorowa gorge to the west and a ring of domes to the east and south of the field. The Olkaria Domes field is a high-temperature field with most of the wells producing two-phase fluid. This report aims at discussing and updating the natural-state model of the Olkaria Domes field reservoir, incorporating data from recently drilled wells. Several 3-D natural-state numerical models of the entire GOGA geothermal system have been developed, the first in 1987 by G.S. Bödvarsson and K. Pruess. Downhole profiles of temperature and pressure in the wells were interpreted to obtain the natural state of the reservoir in the wells' locale. Previous work was incorporated and an inclusive model developed that forms the basis of a simple numerical model for the natural state that could provide the standard, pre-exploitation natural state of the Olkaria Domes field reservoir. In this report, the main focus will be on updating the natural-state model of the Olkaria Domes field, equivalent to the undisturbed formation before exploitation of the resource began. Previous models have been developed, the latest completed in 2012 by the Mannvit/ÍSOR/Vatnaskil/Verkís consortium.

1. INTRODUCTION

The Greater Olkaria geothermal area (GOGA) is one of the most exploited geothermal systems in the world. It is located in the East African Rift system that extends from the afar triple junction at the Gulf of Aden in the north to the south in Beira, Mozambique (Abbate et al., 1995). The rift is part of a continental divergent zone where spreading results in the thinning of the crust and the eruption of lavas and associated volcanic activities (Lagat, 2004). There are two divisions in the East African Rift valley: the Eastern and the Western rift valleys. Geothermal activity is rampant in many areas of the Kenyan rift, which is a segment of the East African Rift that runs from Lake Turkana to Lake Natron in northern Tanzania. There are about fourteen geothermal prospects (Figure 1) that are associated with Quaternary volcanic centres occurring in the axial region of the Kenyan rift (Omenda, 1998). Currently, two geothermal prospect areas are under exploitation for electricity production: the GOGA area and the Eburru geothermal field. In the Menengai geothermal field, drilling activities are currently ongoing in

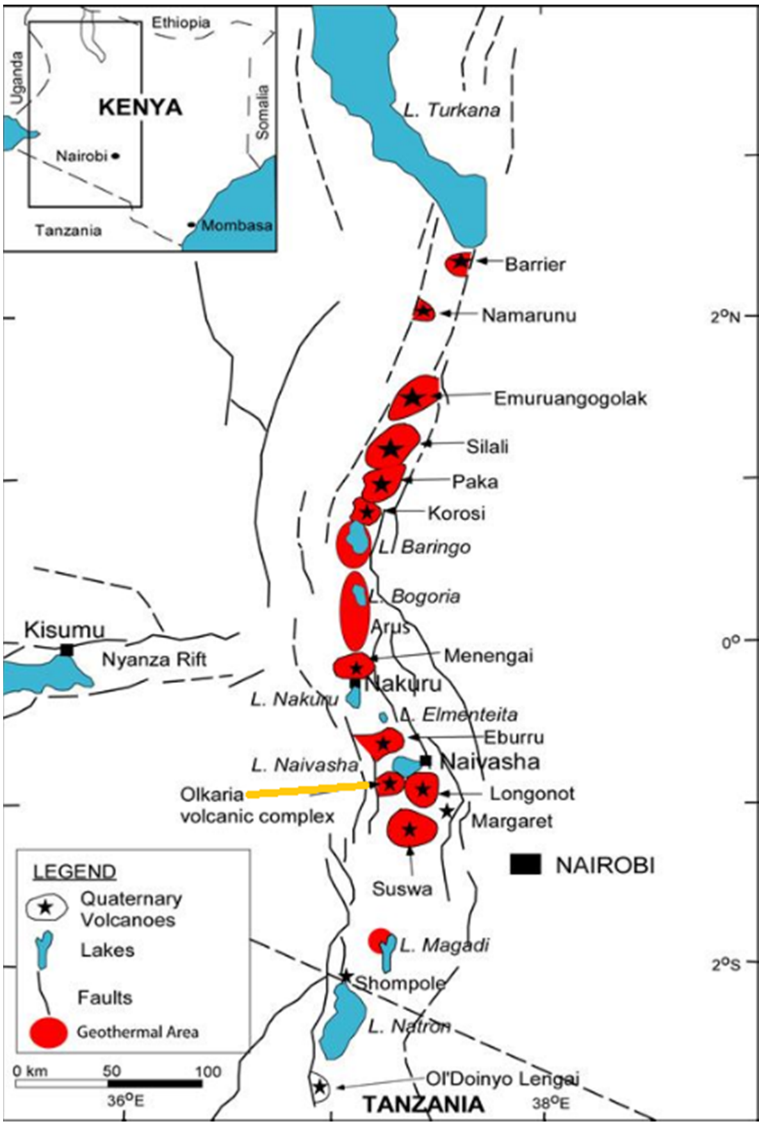

FIGURE 1: Location of Greater Olkaria geothermal area and other volcanic centres in Kenya (Ofwona et al., 2006)

preparation for future exploitation. GOGA is in the southern part of the Kenyan rift, located to the south of Lake Naivasha and roughly 120 km northwest of Nairobi city.

In the 1950s, exploration of geothermal resources in Kenya started with geological surveys in the region between Olkaria and Lake Bogoria in the northern part of the rift. The result was the drilling of two exploration wells, X-1 and X-2, in Olkaria field in which high temperatures were encountered at depth (Kenya Power Company, 1984). The success of these wells lead to further studies including surface exploration and resource capacity assessments. By 1976, six deep wells had been drilled and the field was eventually subdivided into various prospect sectors for easier development. The sectors were named with respect to Olkaria hill as shown in Figure 2.

In 1981 the first 15 MWe generating unit harnessing steam from the Olkaria East field was commissioned. Later, in 1982 and 1985, two additional units (units 2 and 3), each 15 MWe, were commissioned, respectively. Olkaria II, located in the Olkaria Northeast sector, was commissioned in 2003, producing 70 MWe. An additional 35 MWe turbine was commissioned in May 2010, increasing the generating capacity to 105 MWe. Olkaria III, located in the Olkaria West field, currently generates a total capacity of 110 MWe. The first 12 MWe unit at Olkaria III was commissioned in 2000, a second 36 MWe unit was later commissioned in 2009 and the third 52 MWe unit was completed in February 2014. Currently, construction of a fourth 140MWe unit plant in the Olkaria East field is near completion as well as a 140 MWe plant in the Olkaria Domes geothermal field.

2. FIELD REVIEW

2.1 Olkaria Domes field development

KenGen, the state-run power generating company in Kenya, carried out a detailed geo-scientific survey in the Domes sector. The survey undertaken between 1992 and 1997 involved geology, geophysics, and geochemistry as well as heat flow measurements. Analysis of data from this study lead to the siting of three exploration wells, OW-901, OW-902 and OW-903 which were drilled between 1998 and 1999

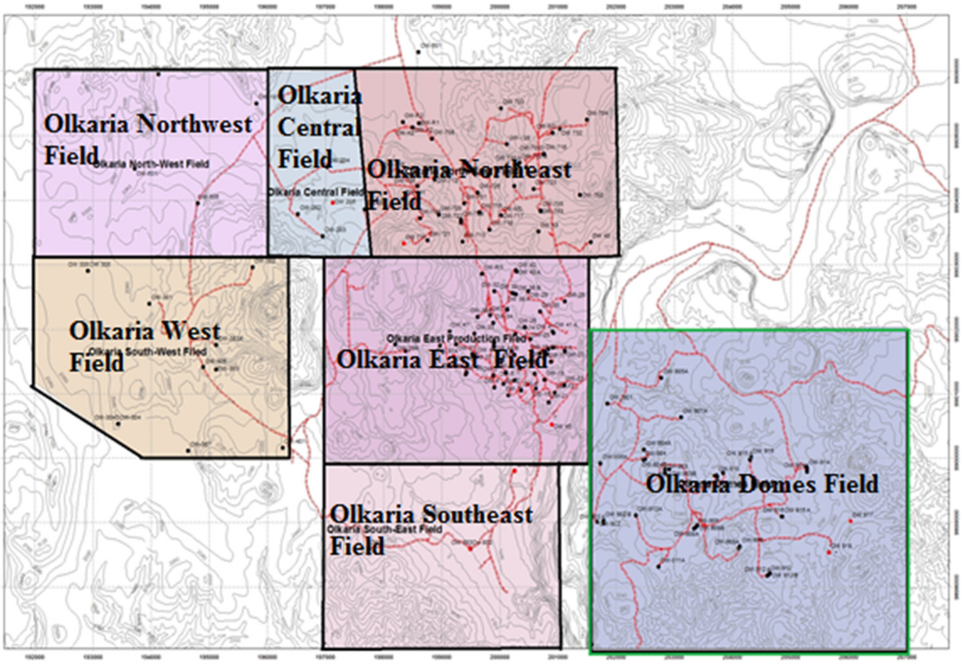

FIGURE 2: Olkaria field subsections

(Lagat, 2004). All three wells were successful and able to discharge steam. Down-hole data from the drilled wells was analysed and additional geophysical surveys were carried out with MT and TEM techniques. The success of the three exploration wells lead to appraisal drilling where six wells were drilled within the field. Since then there have been numerous drilling activities in the field and increased development.

2.2 Geological overview of Olkaria Domes field

Geo-scientific studies conducted over time in the Olkaria field indicate that the field is a remnant of an old caldera complex cut by N-S normal rifting faults that became the centre for later eruptions, forming rhyolitic and pumice domes (Ofwona, 2002). The surface and subsurface rocks are dominated by pyroclastics, tuffs, rhyolites and some basalts which may vary considerably from one place to another. Figure 3 shows the structure within the Greater Olkaria volcanic complex. They include the ring

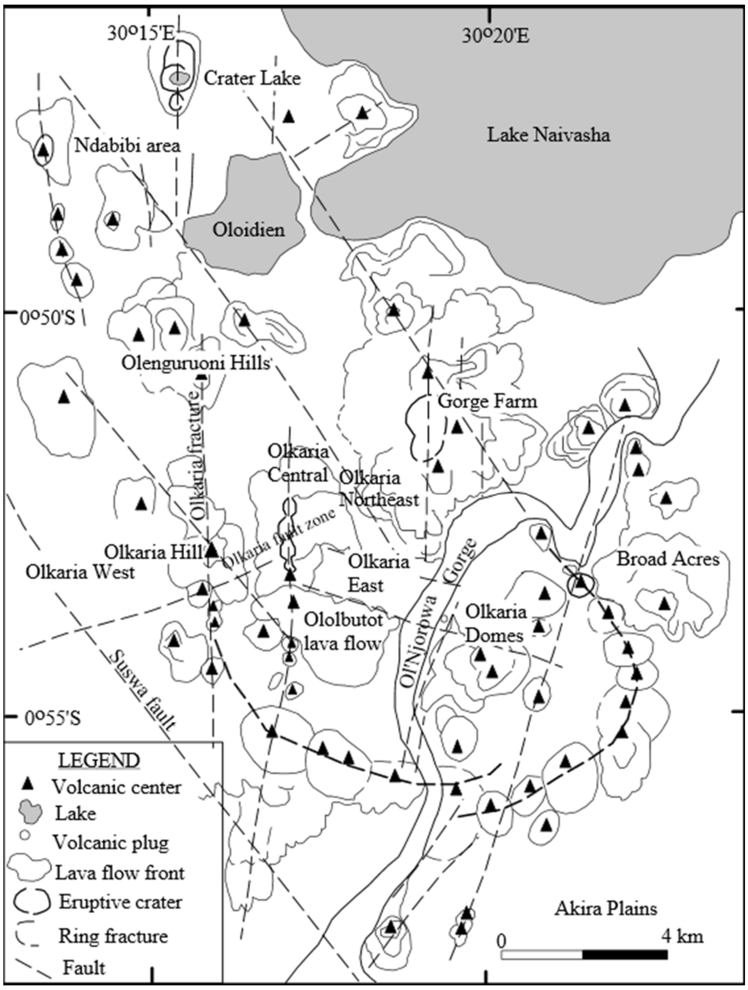

FIGURE 3: Structural map of Olkaria (Lagat, 2004)

structure, the Ol'Njorowa gorge,the ENE-WSW Olkaria fault and N-S, NNE-SSW, NW-SE and WNW-ESE trending faults (Lagat, 2004). In general, faults are very scarce in the Olkaria Domes field but dominate in other parts of the complex. In the Olkaria Domes area there are hydroclastic craters located on the northern part of the field that mark a magmatic explosion edge (Mungania, 1999). The craters form a row over which the extrapolated caldera rim trace (ring structure) passes. The field is also bound by Ol'Njorowa gorge that demarcates the field from the Olkaria East field.

OW-916 is a well drilled in the Olkaria Domes field and exhibits the typical lithology of most of the wells in the field. From Figure 4 we can deduce that the lithology of the Olkaria Domes field is dominated by pyroclastics, tuffs, rhyolites, trachytes and basalts with minor syenite intrusives.

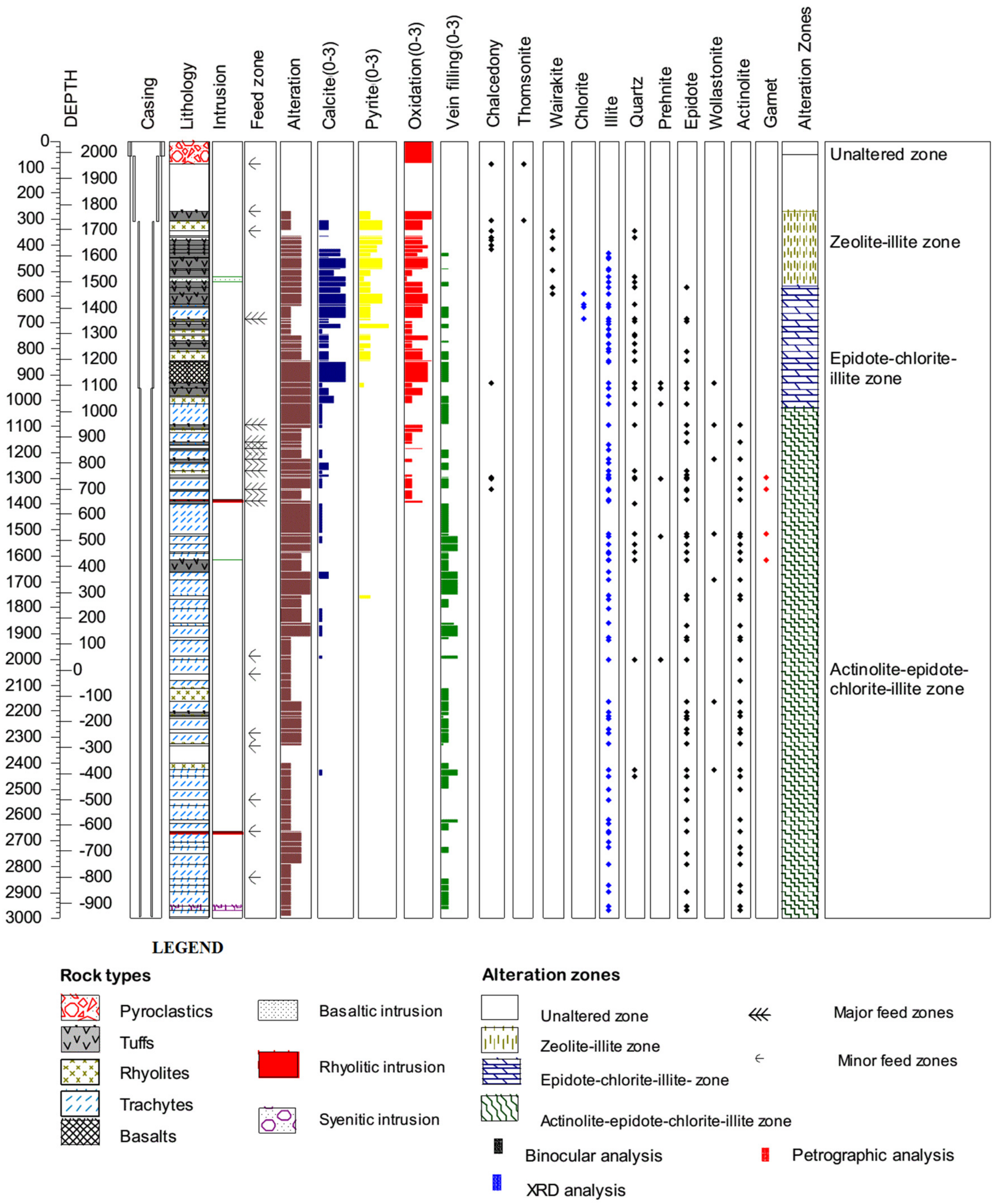

FIGURE 4: Hydrothermal alteration minerals in Well OW-916 (Mwangi, 2012)

2.3 Geophysical overview of Olkaria Domes field

In the analysis based on transient electromagnetic (TEM) and magneto-telluric (MT) soundings, at 0 m a.s.l., the high-temperature alteration (resistive core) dominates in the centre of the Olkaria Domes field (Wanjohi, 2011). In Figure 5 the high-resistivity anomaly of 50–120 Ωm extends over most of the area except in the northern and southern parts. This high-resistivity anomaly can be associated with the dominance of high-temperature alteration minerals (Kandie, 2010) and may indicate an area containing geothermal fluids of relatively high temperatures. Overlying the high-resistivity core is a lower resistivity (<20 Ωm) layer in the northern and southern parts of the field. This could be a zone of high permeability where hydrothermal alteration is not advanced, suggesting a possible up-flow zone beneath (Wanjohi, 2011).

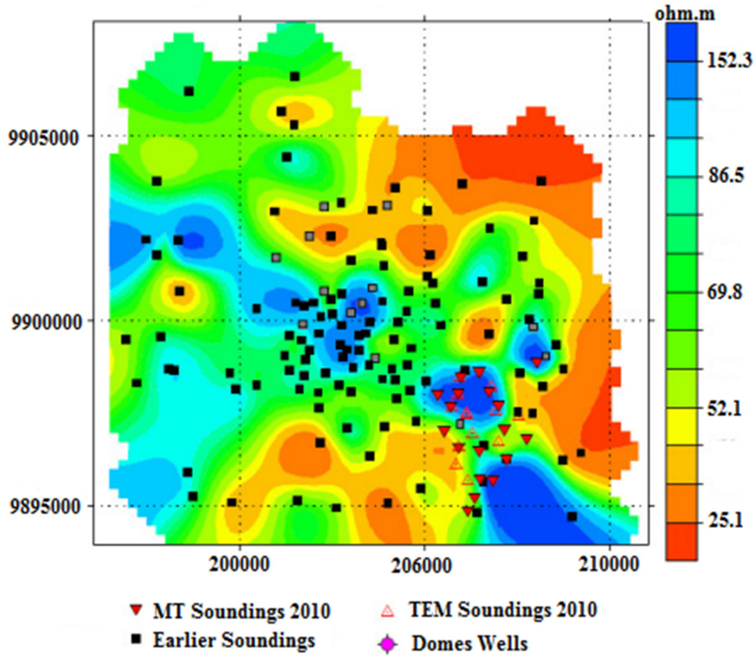

FIGURE 5: Iso-resistivity map of Domes area at sea level (Wanjohi, 2011)

2.4 Geochemical overview of Olkaria Domes

Geothermal fluids in the Olkaria Domes reservoir are bicarbonate in nature and correspond to peripheral waters (Malimo, 2009). The Olkaria Domes fluids seem to plot similarly to those of the Olkaria West and Olkaria Central fields, unlike the wells in the Olkaria East field and in Olkaria Northeast which discharge sodium-chloride type water of a mature nature. Solute and gas geothermometry indicate high temperatures in the range of 250-350°C (Malimo, 2009). Fluid extracted from the Olkaria Domes wells contain low calcium concentrations and high pH. Calcite scaling can be expected to be minimal in these wells but the fluid has to be separated at temperatures above 100°C to prevent silica scaling (Karingithi, 2000). Studies, done by Kamunya et al. (2014), show that wells in the Olkaria Domes field discharge a mixture of chloride and bicarbonate end-member water, as shown in Figure 6. Bicarbonate waters are found in areas to the

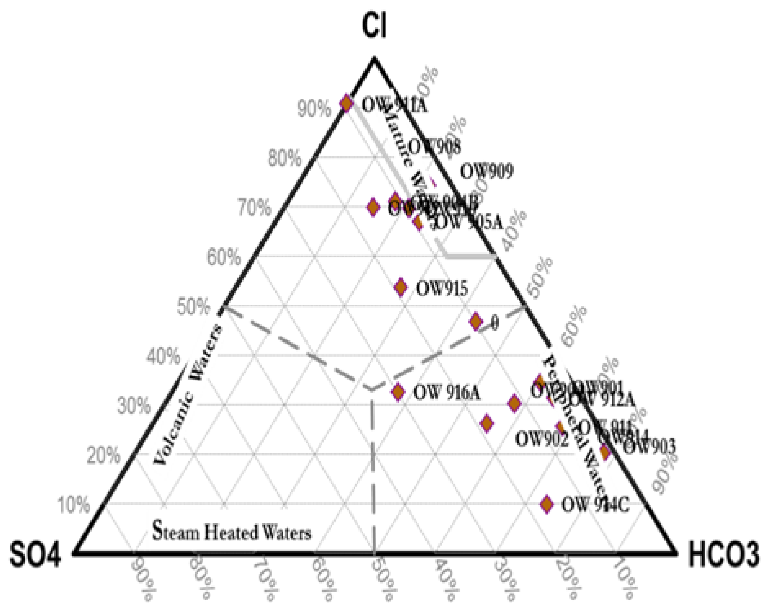

FIGURE 6: Water types of the Domes geothermal area (Kamunya et al., 2014)

northeast and southwest of the Olkaria Domes field. This could be due to the contribution of recharge fluids through the NE-SW faulting and the interpreted buried caldera that forms a concentric series of rhyolitic ash domes in the east, frequently referred to as the ring structure (Kamunya et al., 2014).

2.5 Temperature and pressure in Olkaria Domes geothermal field

Temperature and pressure models have become important tools in the calibration of natural-state models of geothermal systems before exploitation. The temperature plots of a few selected wells in the Olkaria Domes field (Appendix I) illustrate conductive heat flow down to 1000 m depth; below this depth convective flow is dominant. The calculated formation temperature and initial pressure, assumed to be the natural temperature and pressure conditions at the well location, are extrapolated from temperature and pressure measurements for a given well, taking into account the effect of boiling and internal flows. The data obtained is used as a basis for calibration of the numerical model. The location of the wells in the Olkaria Domes field is shown in Figure 7.

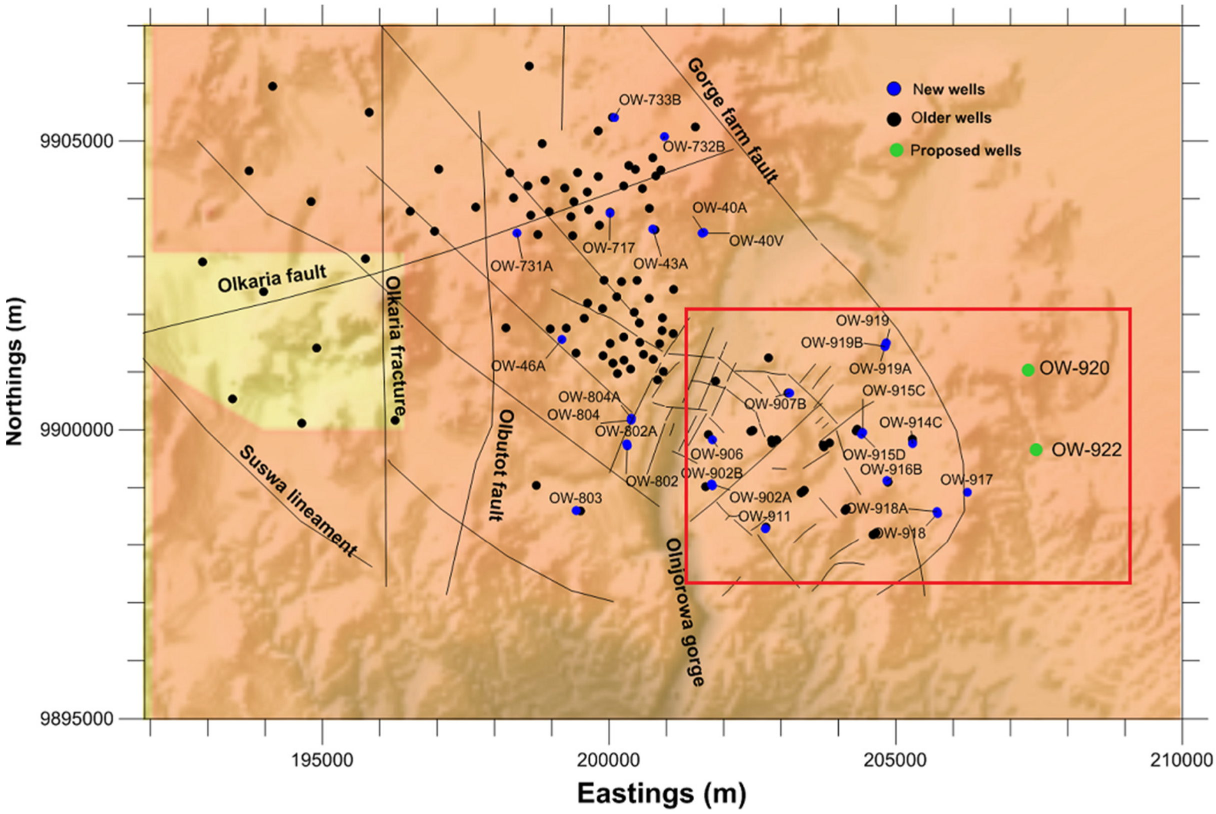

FIGURE 7: Wells in the Greater Olkaria geothermal field;
the red box marks the Olkaria Domes field

Figure 8 shows the estimated formation temperature for Olkaria Domes vertical wells. The plot shows that a majority of the wells have the same characteristic nature of conductive heat transfer from the surface to around 1000 m depth, with convective heat flow below that depth.

A vertical cross-section in the NW-SE direction across the Olkaria Domes field is shown in Figure 9a. From the cross-section, an isotherm map was generated, showing the existence of hot plumes around Wells OW-916A, OW-916B, OW-912A, OW-915A, OW-909A, OW910A, OW-901, OW-921A and OW-904B. These hot plumes of 260°C isotherm reach up to around 1000 m a.s.l. This is also seen in isotherm maps at different depths in Figure 10.

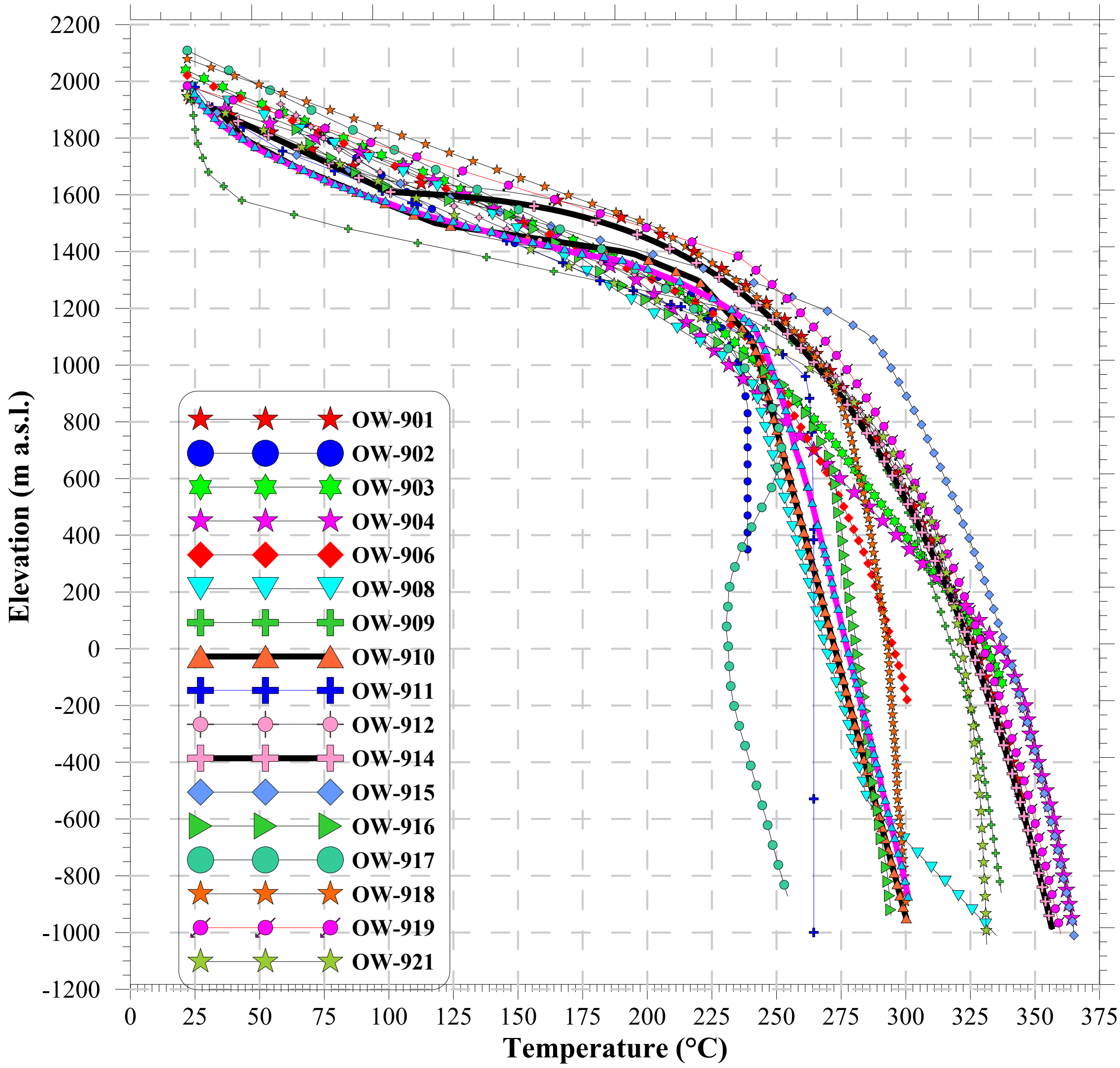

FIGURE 8: Estimated formation temperature plot for Olkaria Domes vertical wells

The isotherms in the southern part of the well field show low temperature around Well OW-911A, and in the southeast and northwest parts of the field they indicate cooling around Wells OW-918A, OW-905A and OW-907B. The isotherms indicate that the main up-flow zone for the Olkaria Domes field is located in the area around Wells OW-914 and OW-915 and eastward. Other minor up-flow zones are observed around Wells OW-901 and OW-904. Slight cooling is observed around Wells OW-910 and OW-916.

Pressure drives the flow of fluids in a reservoir and during production there is usually pressure drawdown in the field. Hence, pressure logging is performed in order to acquire information on the regional geothermal system and determine the initial reservoir pressure before production began (Stefánsson and Steingrímsson, 1980). The pressure logs in the Olkaria Domes wells have been studied and the pressure contours plotted at different depths (Figure 11). High-pressure regions are associated with the upflow zones in the field.

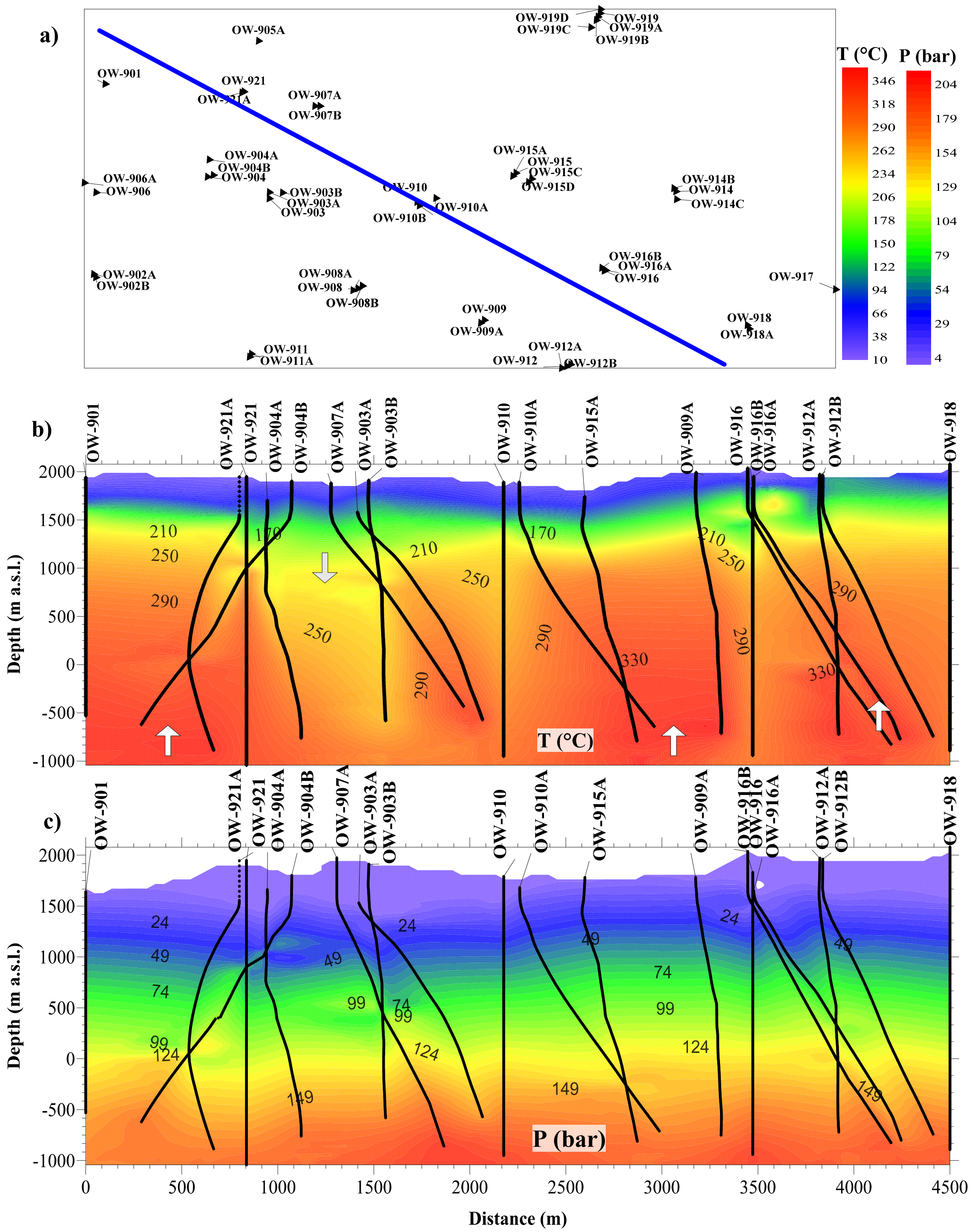

FIGURE 9: NW-SE cross-section; a) location; and vertical contours plotted for b) temperature and c) pressure; arrows indicate estimated direction of flow within the reservoir

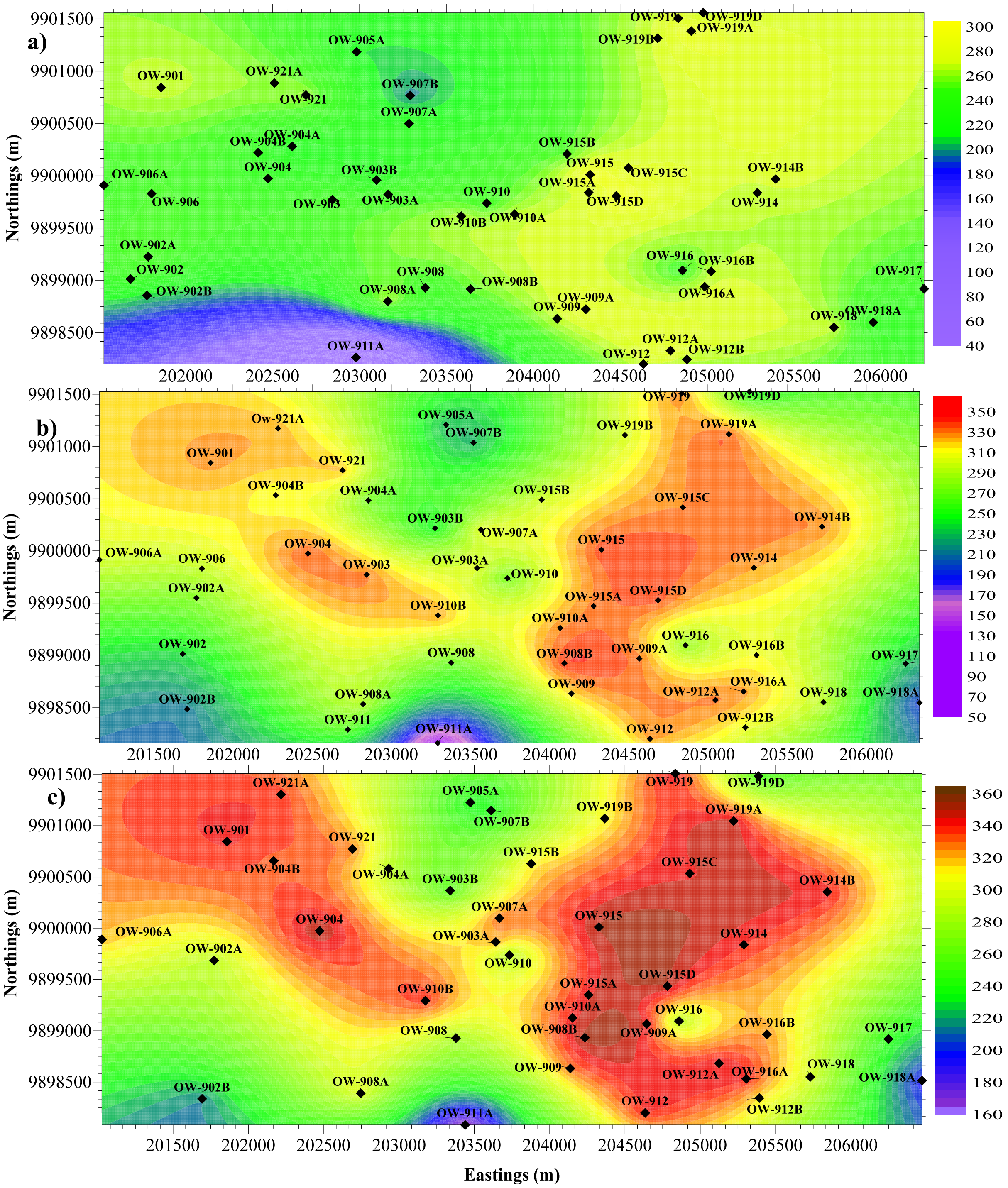

FIGURE 10: Temperature contours at a) 1000 m a.s.l.; b) 0 m a.s.l.; and c) 400 m b.s.l.

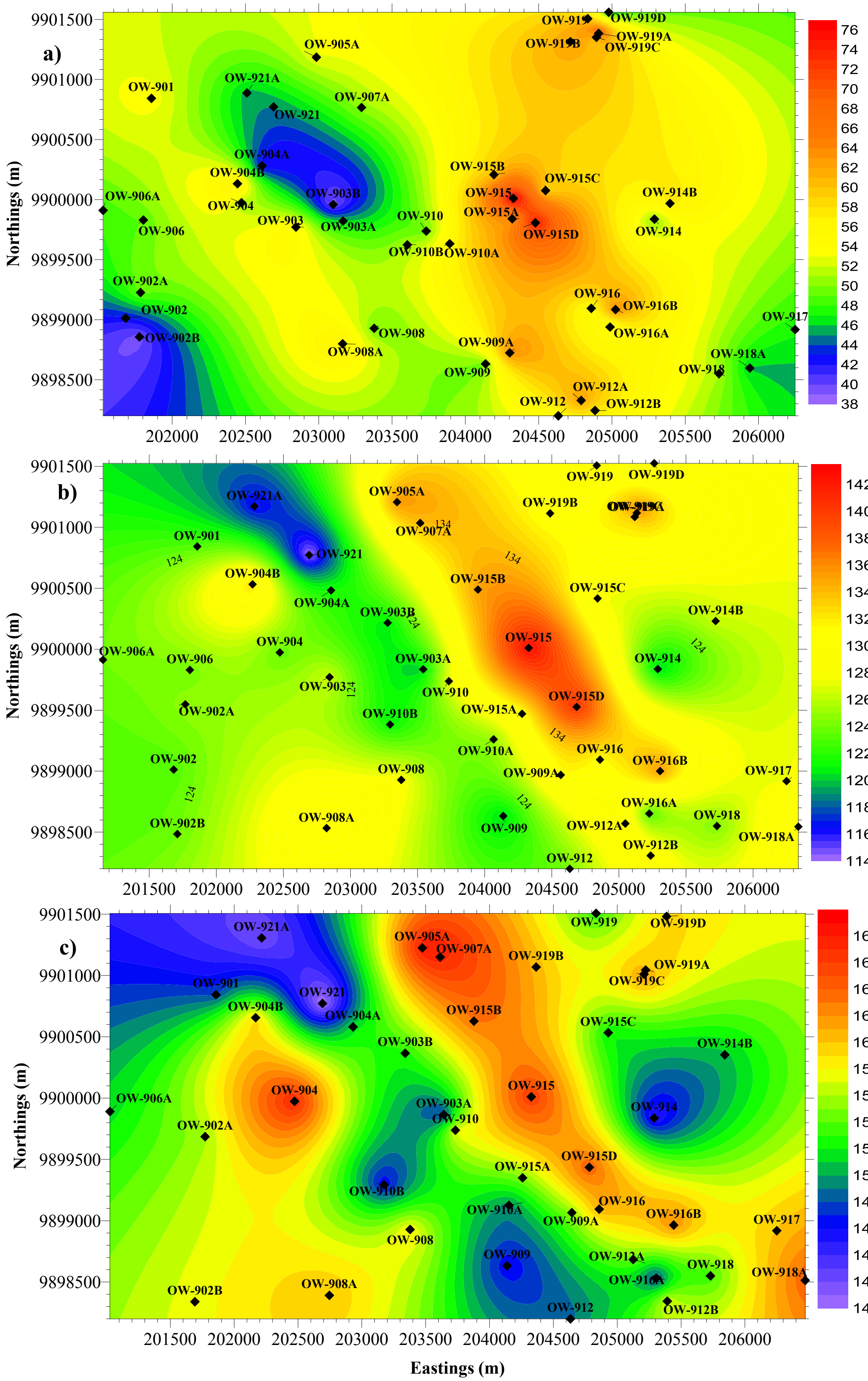

FIGURE 11: Pressure contours at a) 1000 m a.s.l.; b) 0 m a.s.l.; and c) 400 m b.s.l.

3. CONCEPTUAL MODELS

3.1 Fluid and heat flow in hydrothermal systems

Hydrothermal systems are comprised of fluid, heat, and permeability in a naturally occurring geological formation. Geothermal energy is the heat energy kept within the earth's crust and therefore forms the roots of a hydrothermal system. This energy can be accessed through drilling and harnessed using various technologies. The geothermal fluid transports energy from the crust to the surface. Hence, there is transfer of both mass (fluid) and thermal heat that plays a very important role in geothermal energy exploitation. The flow of fluid through porous and fractured media is described by two main equations; the pressure diffusion equation and Darcy's law. Darcy's law describing fluid flow in groundwater systems is given in Equation 1 (Bear, 1979):

$$Q = KA\frac{dh}{dl} \tag{1}$$

Values of K and h can be written in simple form as shown in Equation 2:

$$K = k\left(\frac{\rho g}{\mu}\right), h = \left(\frac{p}{\rho g} + z\right) \tag{2}$$

$$q = \frac{Q}{A} = -k\left(\frac{\rho g}{\mu}\right) * \frac{d}{dl}\left(\frac{p}{\rho g} + z\right) \tag{3}$$

where q is the fluid mass flux vector (kg/s m^2), ρ is the fluid density, μ is the dynamic viscosity of the fluid, g is the gravitational constant, Q is the mass flow rate (kg/s), k is the rock permeability (m^2), p is the fluid pressure (Pa), A is the cross-sectional area through which fluid flows, z is the force in z direction and l is the distance over which flow occurs.

In Equation 3 there are two forces acting in the direction of flow: the net pressure force and gravitational force in the direction of flow. For mass transfer evaluations as well as reservoir pressure changes in geothermal reservoirs, the pressure differential equation is used. It is a combination of mass conservation and Darcy's law for the mass flow. Equation 4 describes storativity, the property of mass extraction that controls how initial pressure changes occur in geothermal reservoirs. This property varies from one rock type to another.

$$\nabla m = \nabla PV\rho_w\{\emptyset c_w + (1 - \emptyset)c_r\} \tag{4}$$

In the above equation, Δm is the change in mass (kg) stored, Δp is the change in pressure (Pa), ρ_w is the density of water, ϕ is the porosity, and c_w and c_r are the compressibility of water and rock, respectively.

In heat flow (thermal flow), a general heat conduction equation is given by:

$$Q = -K \nabla T \tag{5}$$

where Q is the heat flux density (J /s m^2), K is the thermal conductivity of the material (J /s °C.m) and ∇T is the temperature gradient. Using Fourier's law combined with the principle of conservation of energy, Equation 6 can be derived:

$$\rho\beta\frac{dT}{dt} = \nabla (K\nabla T) + M_\rho \tag{6}$$

where ρ is the density, β is the heat capacity (J /kg °C) of the material, M is an immersed heat source/sink density (J /s kg), ∇T is the temperature gradient, t is the time and K is the thermal conductivity of the material.

Since the process of heat transport through permeable media in geothermal systems involves heat conduction through the rock matrix, fluid percolation through pores and fracture and heat transfer between the fluid and the rock matrix, an equation of heat transport can be deduced (Axelsson, 2012):

$$< \rho\beta > \frac{dT}{dt} = -\beta_w \rho_w \mu \nabla T + \nabla.(K\nabla T)\,) \tag{7}$$

where ρ_w is the density of water, β_w is the heat capacity (J /kg °C) of the water, ∇ T is the temperature gradient, t is the time, K is the thermal conductivity of the material, $<\rho\beta>$ is the heat capacity of the rock matrix and μ is the dynamic viscosity of the fluid.

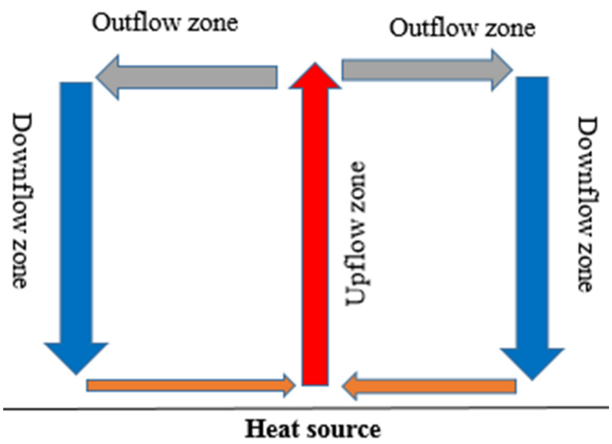

FIGURE 12: Flow characteristics within a cell

In natural-state geothermal systems, free convection is the most common heat transfer process. Due to variations in temperature in geothermal systems, buoyancy forces are produced as a result of variation in density. As meteoric water percolates beneath the earth, it is heated at great depths and rises back up to the surface, causing flow against the decreasing pressure gradient direction. This can be compared to a flow through a single cell (Figure 12).

The flow characteristics within a cell can be summarized by combining Equations 1, 4 and 7 and simplifying them into one function called the Rayleigh number:

$$R_a = \frac{\beta_w \rho_w g c_w \nabla T k h}{\upsilon K} \tag{8}$$

where R_a is the Rayleigh number, g is gravitational acceleration, c_w is the thermal expansion coefficient for water, k is rock permeability, β_w is the heat capacity of the fluid, ∇T is the temperature difference over a given distance, h is the thickness of the reservoir, ρ_w is the density of water, K is the thermal conductivity of the material and υ is the kinematic viscosity.

This number is used to estimate conditions for the development of a natural-state hydrothermal system. It gives the ratio of buoyancy forces to viscous resistance. For convective flow in a saturated aquifer, $R_a > 4\pi^2$ known as the critical Rayleigh number and the value normally ranges from 100 to 1000 in geothermal systems (Ofwona, 2002). Before exploitation, the initial fluid circulation in the hydrothermal reservoir is controlled by the dynamic balance of mass and heat but, during exploitation, fluid flow is controlled by the pressure gradient created by the discharging well.

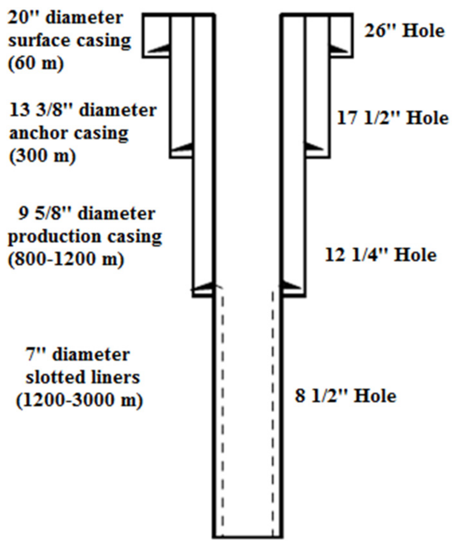

FIGURE 13: Casing design for most Olkaria Domes wells

3.2 Characteristics of Olkaria Domes wells

Unlike most of the wells in other Olkaria fields, wells in the Olkaria Domes field consist of 20" diameter surface casing down to a depth of 60 m, followed by 13 3/8" diameter anchor casing down to 300 m depth, followed by 9 5/8" diameter production casing down to 800-1200 m depth and finally 7" diameter slotted liners in the production hole (Figure 13). Temperature and pressure logs in the wells indicate that most wells have traversed multiple permeable zones (Figure 14). Due to an overall good permeability of the formation, most of the wells are very good producers. The formation permeability influences the ability of fluid to flow through the feed zones to the well, hence determining the inflow performance.

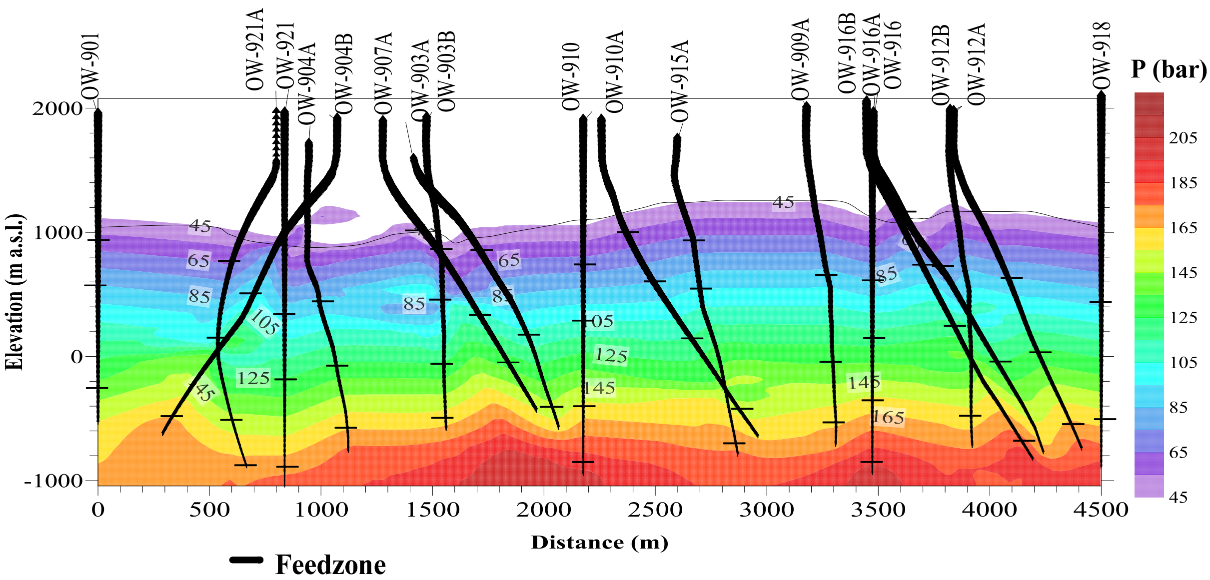

FIGURE 14: Pressure isobars with 50 bar isoline from 1000 m

The discharge test results obtained from discharging Olkaria Domes wells indicate that the fluid from the reservoir is two-phase fluid with high enthalpy. An enthalpy iso-map is shown in Figure 15; the eastern part of the field registers high enthalpy values compared to the western part of the field. This is in agreement with temperature contours and indicates that this eastern region is an up-flow zone within the field.

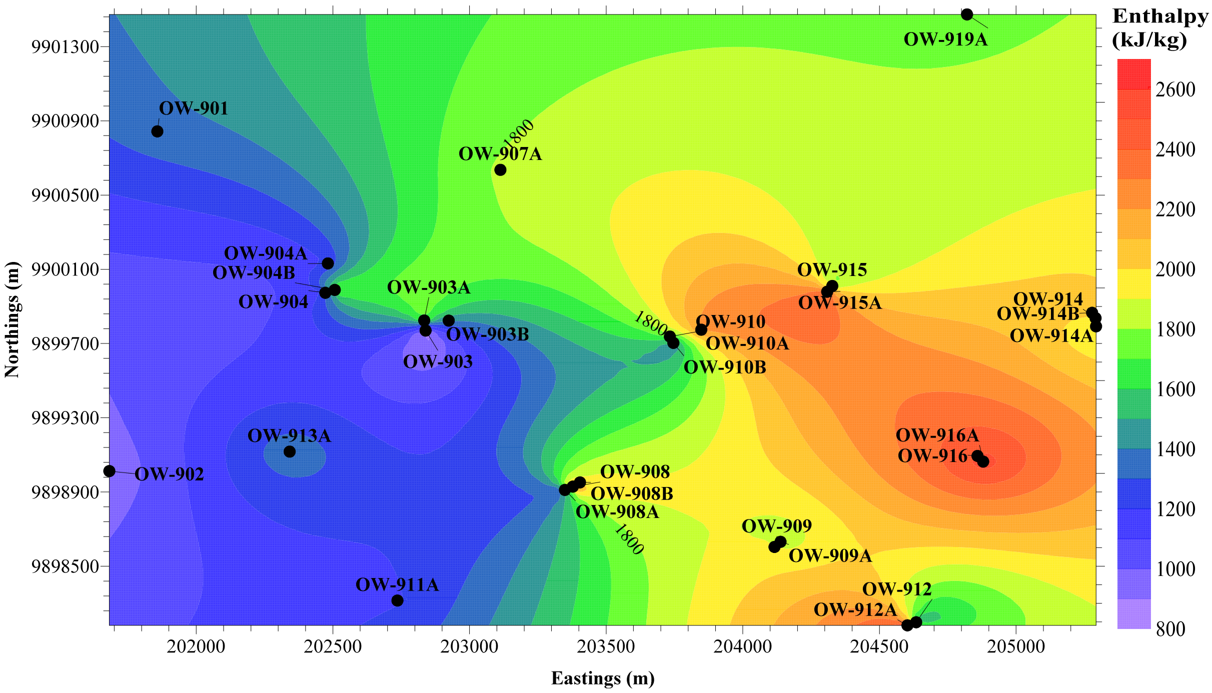

FIGURE 15: Enthalpy distribution in the Olkaria Domes field

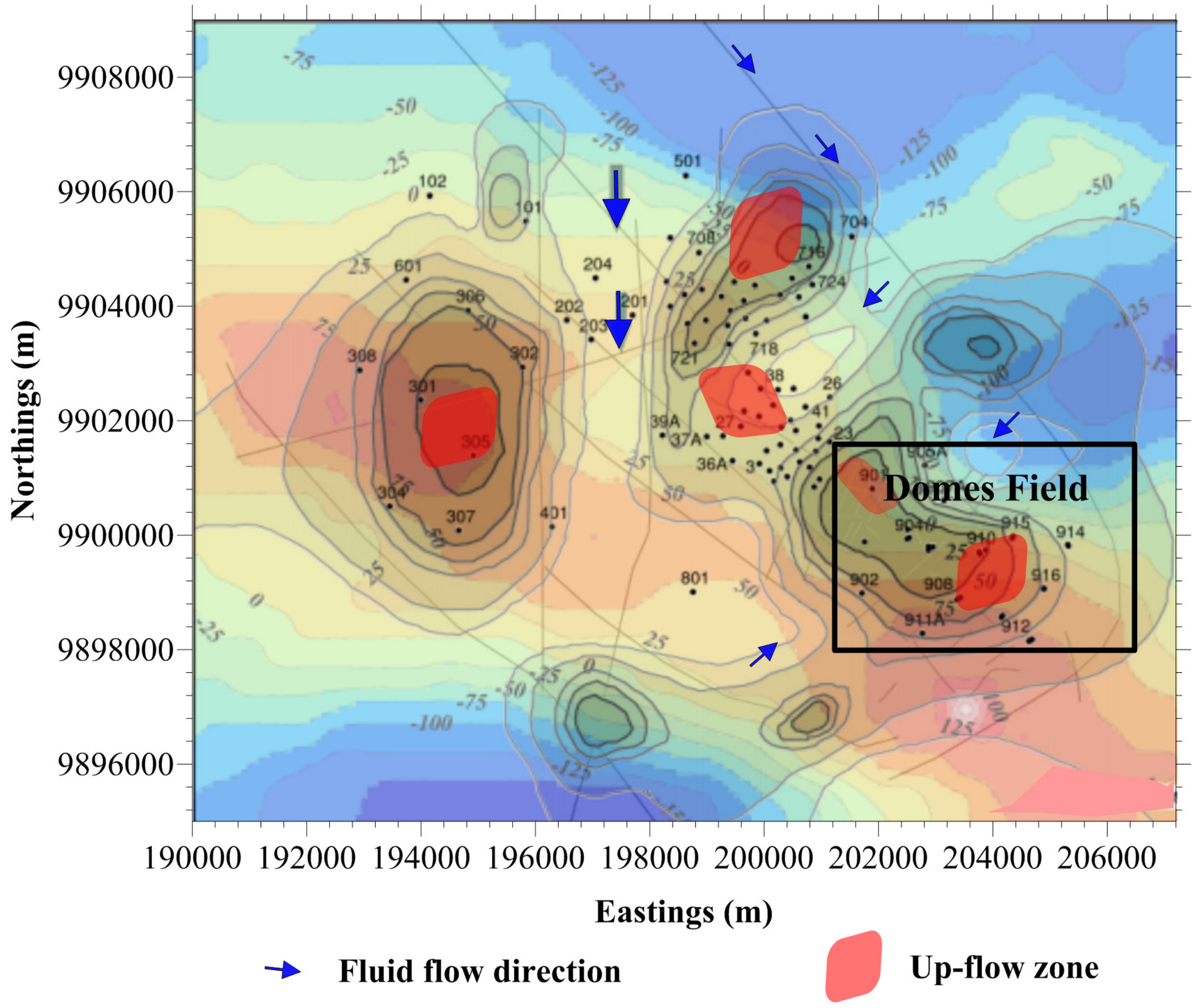

FIGURE 16: Conceptual model with up-flow zones in the Greater Olkaria geothermal area

3.3 Conceptual models of the Domes field

Conceptual models are important in field developmental plans, including selecting the locations and targets of future wells. They are descriptive or qualitative models incorporating and unifying the essential physical features of the systems (Grant et al., 1982). They are created using the analysis of geological and geophysical information, temperature and pressure data, as well as information on the chemical content of reservoir fluids. Through the use of conceptual models, resource assessment can be made including volumetric assessments and numerical modelling. The conceptual model of the GOGA area has been constantly updated and developed in past years (Mannvit/ÍSOR/Vatnaskil/Verkís Consortium, 2011). A simple conceptual model that describes the location of the heat source and features of the hydrological system within the entire Olkaria field is represented in Figure 16. One up-flow zone exists beneath the ring structure in the southeast corner of the Olkaria Domes field, related to the magmatic body evident beneath the area. This magmatic body is located in the centre of the Olkaria Domes area, while the up-flow zone is located in the southeast part of the area. Fracture-controlled permeability related to the ring structure could explain why the up-flow to the Olkaria Domes system is offset southeast of the heat source. The up-flow to the Eastern field and northwest part of the Olkaria Domes field could also be related to the magmatic body beneath the Olkaria Domes area, as well as the body beneath the Eastern field (Mannvit/ÍSOR/Vatnaskil/Verkís Consortium, 2012).). For the purpose of this study, a simple conceptual model based on temperature information for Olkaria Domes is presented schematically in Figure 17.

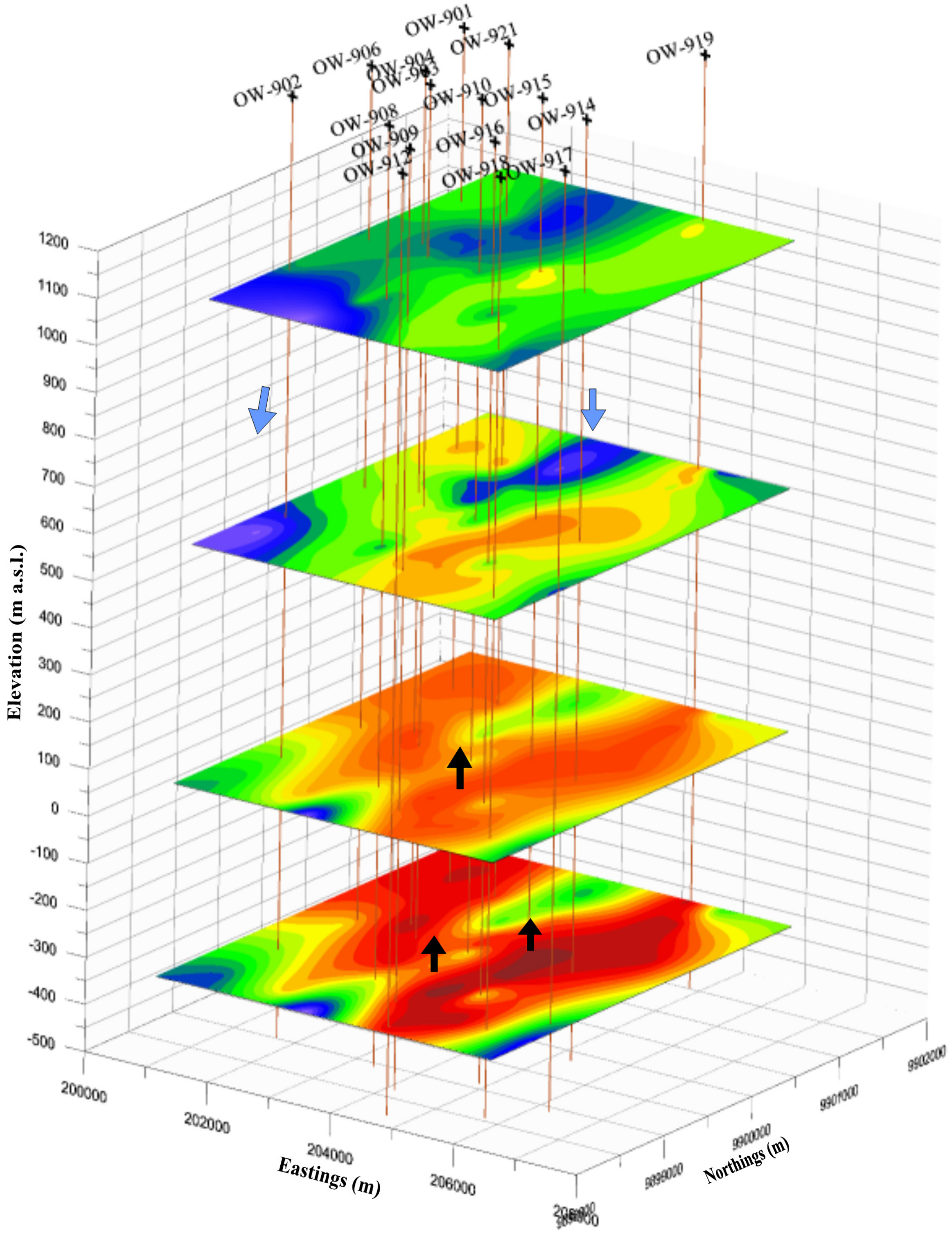

FIGURE 17: Simple conceptual model showing the location of up-flow zones (black arrows) in the Olkaria Domes area

4. NUMERICAL MODELLING

4.1 Theoretical review

TOUGH2 (Transport of Unsaturated Groundwater and Heat) is a general purpose numerical simulator used for modelling non-isothermal flow of multi-component, multi-phase fluids in one, two and three-dimensional porous and fractured media. It is mainly applied in geothermal reservoir studies, nuclear waste isolation studies, environmental assessment and remediation, and flow and transport in variably saturated media and aquifers (Pruess et al., 1999). The simple mass and energy balance equations solved by TOUGH2 can be written in general form as shown in Equation 9.

$$\frac{d}{dt}\int_{V_n} M^K dV_n = \int_{\Gamma_n} F^k \,.\, n\, d\Gamma_n + \int_{V_n} q^k dv_n \qquad (9)$$

where F = Mmass flux;
q = Sinks and sources;
n = Normal vector on the surface element, pointing inwards into Γ_n;
M = Mass per volume.

In Equation 9, the rate of change of fluid mass in V_n is equal to the net inflow across the surface Γ_n plus the net gain from the fluid sources.

Generally, TOUGH2 solves governing equations for the conservation of energy and mass using an integral finite volume structure on both regular and irregular grids. In the preceding sections, fluid flow was described with a multi-phase extension of Darcy's law and heat flux carried by both conduction (Fourier's law) and fluid convection. In a fluid mixture, there are several equations of state that can provide thermo-physical properties of the fluid depending on the characteristics of the system. TOUGH2 can handle sample problems for different equations of state as well as phase transition in the system and diffusion between different phases (Pruess et al., 1999).

When developing a model, the entire volume of the geothermal system is divided into numerous grid elements. The elements are designed in such a manner that each element or group of elements is assigned different hydrological and thermal properties using the conceptual model as a guide. To solve relevant equations for conservation and flow of heat and mass, both finite difference and finite element methods can be used in simulation for natural inflow and outflow in the system (Axelsson, 2013).

4.2 Previous numerical models

Several 3-D natural-state numerical models of the entire Olkaria geothermal system have been developed over the years; the first one in 1987 by G.S. Bödvarsson and K. Pruess. The model focussed on the natural state of the Olkaria geothermal system, deducing that the natural recharge to the system amounted to about 600 kg/s, mainly from the Olkaria East field and partially from the Olkaria Northeast and West fields (Bödvarsson and Pruess, 1987). After several updates from different studies, Ofwona (2002) updated the 1987 model on the basis of both new well data and an additional decade of monitoring data. The same grid was used with an area of about 110 km^2 and a thickness of 1550 m. From his model, it was concluded that the natural state of the system could be simulated by 565 kg/s hot recharge distributed between the western and eastern parts of the Olkaria system, with two up-flow zones in the Northeast sector and one in the East sector. He also concluded that the Olkaria geothermal system is an open system with pressure draw-down confined to production zones (Ofwona, 2002). More recent work was done 2011 and 2012 by a Consortium composed of the Icelandic companies: Mannvit, ISOR, Vatnaskil and Verkís. Their updated model consisted of a grid that covered an area of 720 km^2 and a thickness of 3600 m. The model depth ranges between 1900 m a.s.l. and 1700 m b.s.l. and has 15 layers, each containing 2463 elements. The model was designed using the TOUGH2/iTOUGH2 code which is extensively used in modelling liquid-dominated reservoirs all over the world. From the model it was concluded that the natural state of the system could be simulated by providing sources with just over 200 kg/s of fluids with an average enthalpy of 1600 kJ/kg.

4.3 An update to the existing 3D natural-state model of the Olkaria Domes field

4.3.1 General approach

For the purpose of this study, the most recent numerical model of the entire Olkaria geothermal field, created from the ongoing cooperation between the Mannvit/ÍSOR/Vatnaskil/Verkís consortium and KenGen team, was used. The new wells in the Olkaria Domes field were incorporated into the model in order to update the natural-state model of the field. The horizontal mesh grid for the entire Olkaria system (Figure 18) covers an area of 720 km^2 and covers a depth range from about 2000 m a.s.l. to 1700 m b.s.l. The mesh consists of 36,945 elements and 144,597 connections. The mesh grid has scarce elements near the boundary but becomes dense at the centre of the geothermal system. This is because at the centre of the geothermal system, thermodynamic variable gradients are likely to be greater (in space and time). The top and bottom layers are inactive with 4940 elements. They are set inactive so as to restrain the temperature and pressure gradients in the model, hence conserving a constant temperature and pressure in the top and bottom layers while limiting fluid flow into or out of the adjacent layers.

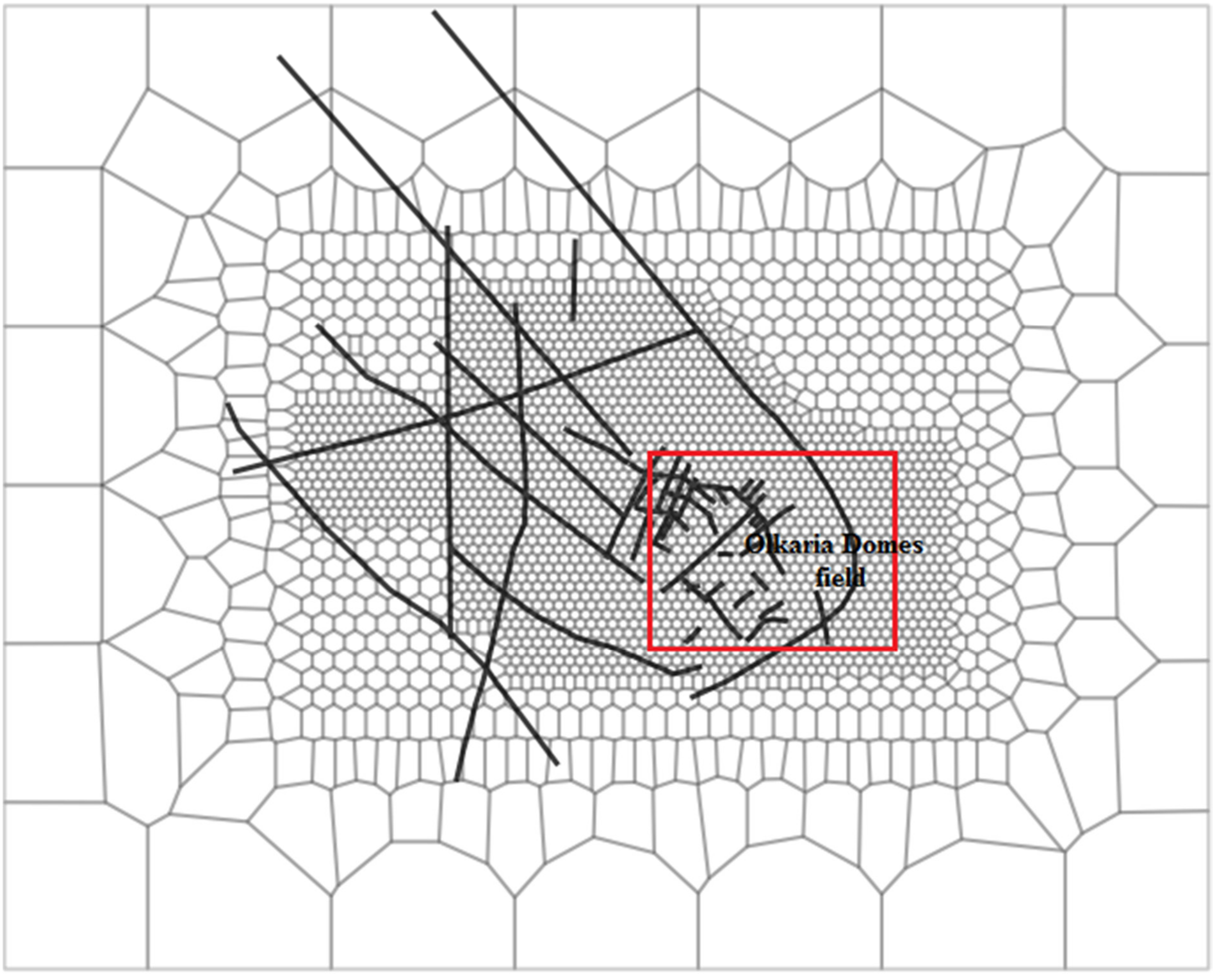

FIGURE 18: The numerical model mesh grid of GOGA (Mannvit/ÍSOR/Vatnaskil/Verkís Consortium, 2012); the red box marks the Olkaria Domes field

The vertical view of the model consists of a total of 15 layers. The top 13 layers are 200 m thick and the bottom two layers are 400 m thick (Figure 19). Layers B and P represent the top and bottom layers, respectively, and both layers are inactive.

There are several different rock types assigned to the elements in the model. Distribution of the rock types was determined by the hydrological flow patterns in the field (as observed in the temperature and pressure logs). Figure 20 shows the distribution of rock types in the numerical model. There are 31 rock types in the entire model. An assumption is that all the rock types have the same physical properties such as density, thermal conductivity and specific heat capacity but with different permeability and porosity (Table 1). Different permeability in horizontal and vertical directions is assigned for different rock types but is the same in the y direction. Porosity and permeability values ranged between the lowest permeable to highest permeable rock types, as shown in Table 1.

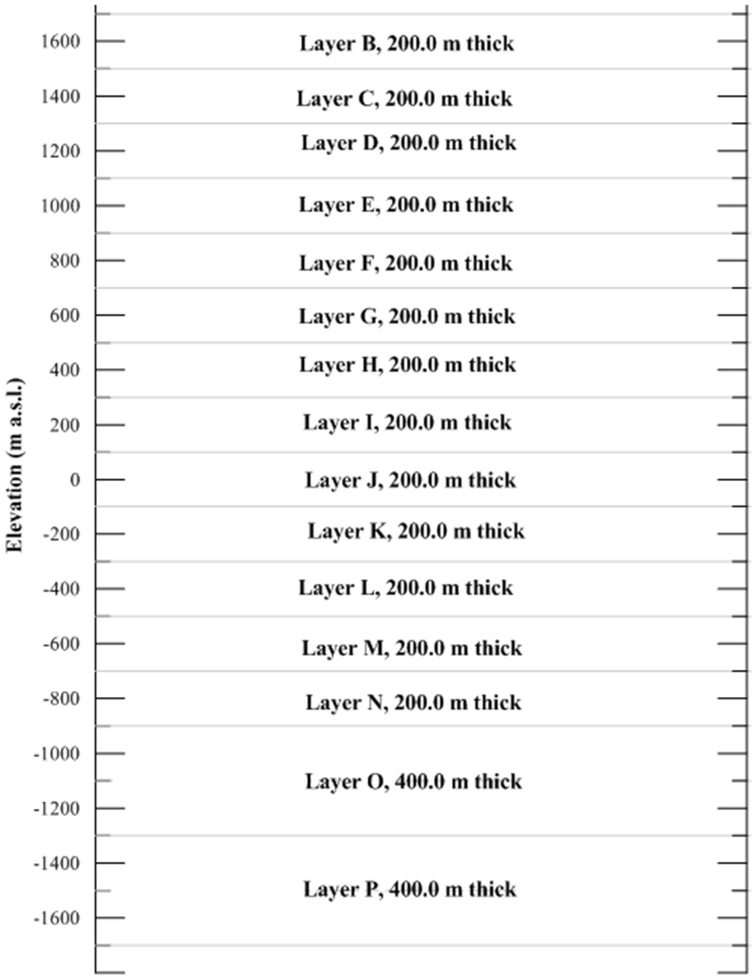

FIGURE 19: Vertical view of the numerical model mesh for the Olkaria geothermal system, showing layer names and thicknesses

TABLE 1: Physical properties for rocks in the numerical model of the Olkaria Geothermal system

Rock physical properties		**Permeable rock**	**Low permeability rock**
Density (kg/m^3)		2650	2650
Specific heat capacity (kJ/(kg.K))		860	860
Thermal conductivity (W/(m°C))		2.0	2.0
Permeability (mD):	Horizontal	0.204	0.0479
	Vertical	2.472	0.0026
Porosity (%)		15	8

4.3.2 Changes made using the current model and discussion

Injection rates and enthalpy values of the sources were adjusted gradually until there was no more change in the model results. A heat source was introduced in element (OB459) to account for the high temperature in the wells around this region. From the temperature isotherm map (Figure 10), a conspicuously low temperature is noted in the field around Wells OW-905A, OW-907B and OW-903B.

To improve the fit in the model, new rock types and a cold source were added to the model (Figure 20). A rock type called BARIA with low permeability was introduced as a barrier that hinders flow of fluid

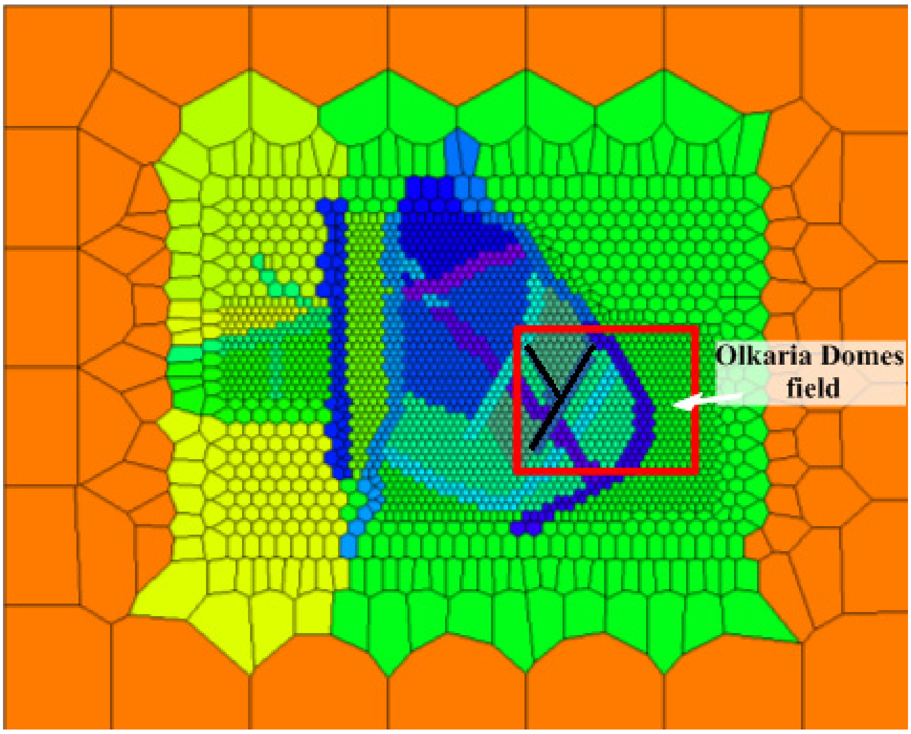

FIGURE 20: Distribution of rock types within the reservoir; black line is the BARIA rock type (modified from Mannvit/ÍSOR/Vatnaskil/Verkís, 2012)

between the up-flow zone and the cold region. The barrier reduces the flow of heat and mass to the cold region and also reduces the low-enthalpy fluid flow across to the up-flow zone. Some wells indicated a temperature inversion at the bottom of the reservoir, hence, the permeability of rock type EBCL in layers M and N was progressively adjusted until an improved match between simulated and observed data was achieved. In general, the permeability distribution and the strength of the mass and heat up-flow into the system were adjusted and the model was then re-run until a reasonable match between the calculated and measured data was reached. Table 2 shows the final calibrated properties of the sources defined in the model.

TABLE 2: Properties of sources

Properties	Hot source	Cold source
Flow rate (kg/s)	70.80	5.78
Average enthalpy (kJ/kg)	1640	950

4.3.3 Results and discussion

Appendix II shows graphs of pressure and temperature calculated by the calibrated model compared with estimated formation temperatures. The model calculations fit the measured data well for most of the wells. An exception, however, is observed in areas within low-temperature zones. Some changes were made in the model so as to obtain a reasonable fit around these areas. This included introducing a barrier rock type and a cold source. Other modifications included changing the rate of mass and heat flow into the system as well as permeability changes. Calculated temperature and pressure contours are presented in Figures 21 and 22. The temperature contours closely match with temperature contours obtained from measured data but for pressure there is a bit of mismatch between the two.

Figure 23 shows the downhole temperature and pressure calculated by the model as a function of the estimated formation temperature and pressure. For a perfect match, the points should fall into some trend of a straight line. The spread of the points gives an idea of the quality of the fit of the model.

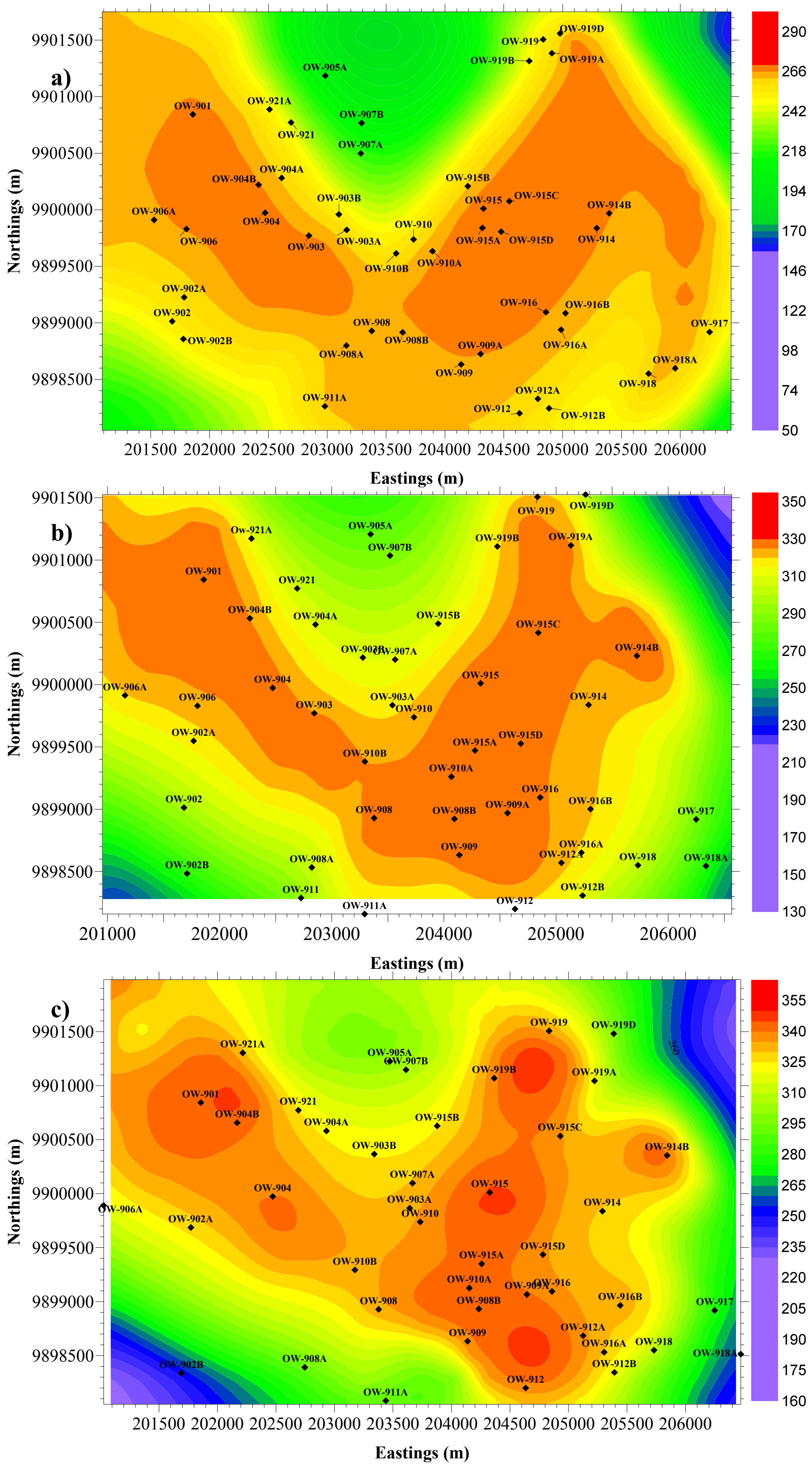

FIGURE 21: Calculated temperature contours:
a) Layer E; b) Layer J; c) Layer L

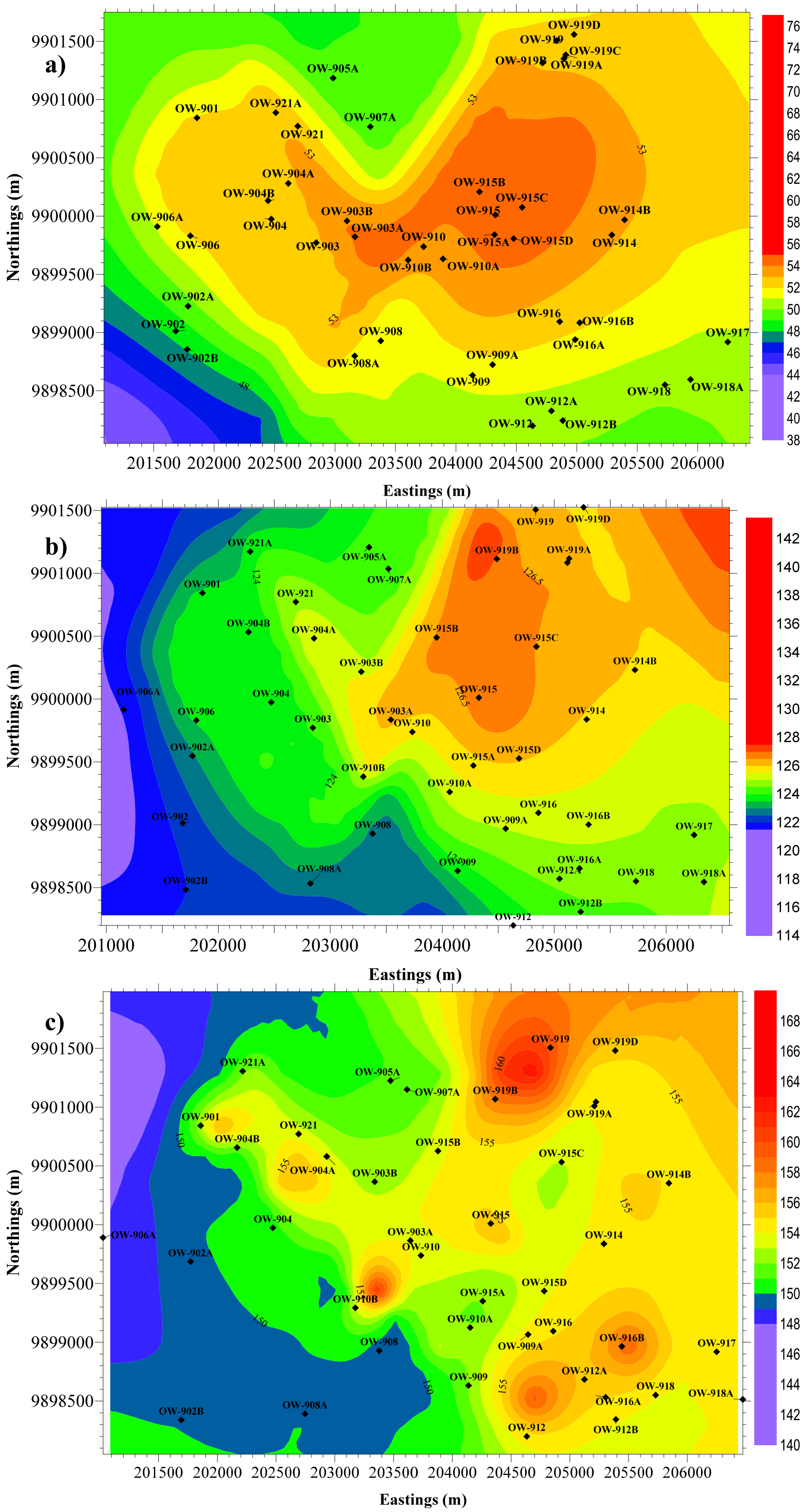

FIGURE 22: Calculated pressure contours:
a) Layer E; b) Layer J; c) Layer L

5. CONCLUSIONS AND RECOMMENDATIONS

The Olkaria Domes reservoir can be classified as a convective cell with a magmatic intrusion in the central part of the field. Associated with the magma intrusion is the major up-flow zone in the southeast part of the field and a minor up-flow zone in the northwest part of the field. From the temperature and pressure models, these up-flow zones are manifested as hot plumes and surrounded by cold down-flow zones. This type of convection flow within the reservoir indicates good recharge to the system.

The major up-flow zone in the field extends all the way to the eastern part of the field. An initial study concluded that the up-flow zone was in the southeast part of the field. But from the research presented here, the zone extends to the eastern part of the field.

To obtain the best match, Olkaria Domes field can be simulated for natural state by an injection of a total mass of about 71 kg/s and enthalpy of 1650 kJ/kg of water. To acquire a better match between the measured values and the calculated model in the region of local cooling around Wells OW-907A and OW-905A, a cold source of 5.78 kg/s and enthalpy of 950 kJ/kg is introduced.

From the cross-sectional temperature plot, one can see that hot plumes are surrounded by cold down flow zones. This is an indication of good recharge to the system.

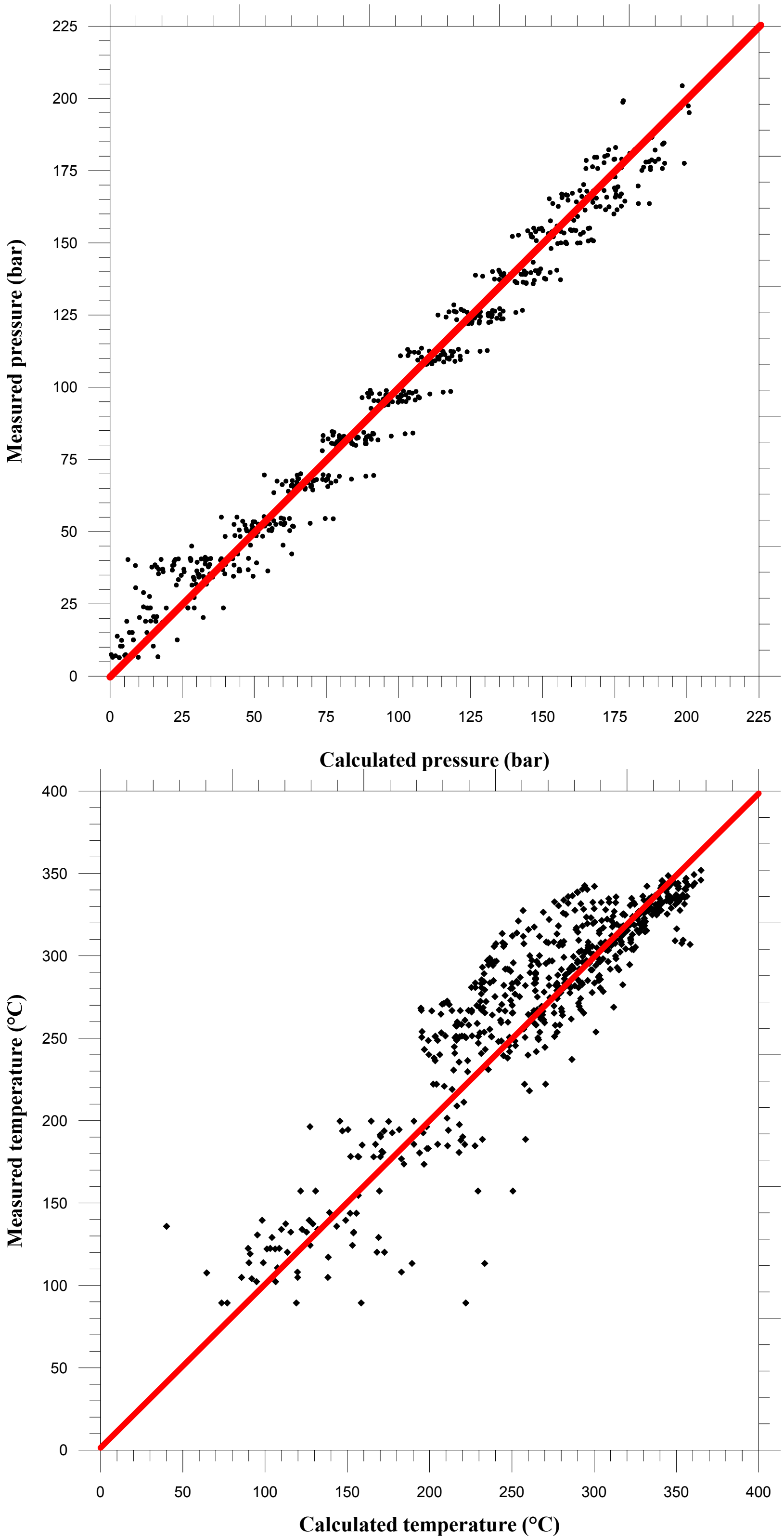

FIGURE 23: a) Downhole pressure calculated by the model as a function of estimated formation pressure; b) Downhole temperature calculated by the model as a function of estimated formation temperature

The model should be updated to include Well OW-922 which was recently drilled outside the ring structure. This would help to delineate the possible extent of the resource outside the ring structure.

And perhaps one or two wells should be drilled north of Well OW-907B to measure the extent of the local cooling in the area.

ACKNOWLEDGEMENTS

My sincere gratitude goes to Mr. Lúdvík S. Georgsson, the Director of the UNU Geothermal Training Programme for the opportunity to take part in the Programme, the Deputy Director, Mr. Ingimar Gudni Haraldsson, for his help and support, Ms. Thórhildur Ísberg, Mr. Markús A.G. Wilde and Ms. Málfrídur Ómarsdóttir for their great support during my study and stay in Iceland, to the staff of UNU, Orkustofnun and ÍSOR, to my supervisors, Dr. Andri Arnaldsson from Vatnaskil Consulting Engineers and Ms. Saeunn Halldórsdóttir from ISOR, for their diligent assistance and advice during my research project, to my employer, the Kenya Electricity Generating Company Ltd. for the chance to attend the training, and to the UNU fellows: thank you for the magnificent time and discussions we shared.

Thanks to my wonderful mother for her love and encouragement, and my sister Phanice for the great support. Finally, I thank God for His sufficient grace that made the programme possible.

REFERENCES

Abbate, E., Passerini, D., and Zan, L., 1995: Strike-slip faults in a rift area: A transect in the Afar Triangle, East Africa. *Tectonophysics, 241*, 67-97.

Axelsson G., 2012: The physics of geothermal energy. In: Sayigh, A. (ed.), *Compreh. Renew. Energy, 7,* 3-50.

Axelsson, G., 2013: Dynamic modelling of geothermal systems. *Paper presented at "Short Course V on Conceptual Modelling of Geothermal Systems" organised by UNU-GTP and LaGeo, Santa Tecla, El Salvador.* UNU-GTP, CD-16, 21 pp.

Bear, J., 1979: *Hydraulics of groundwater.* McGraw-Hill, Inc., NY, 569 pp.

Bödvarsson, G.S., and Pruess, K., 1987: *Numerical simulation studies of the Olkaria geothermal field.* Kenya Power Company, Ltd., internal report.

Grant, M.A., Donaldson, I.G., and Bixley, P.F., 1982: *Geothermal reservoir engineering*. Academic Press, New York, 369 pp.

Karingithi, C.W., 2000: Geochemical characteristics of the Greater Olkaria geothermal field, Kenya. Report 9 in: *Geothermal training in Iceland 2000.* UNU-GTP, Iceland, 165-188.

Kamunya, M.K., Wafula, E., and Wamalwa, R., 2014: *Update of the Olkaria geochemical conceptual model.* KenGen, Kenya, internal report.

Kandie, J.R., 2011: *Geology report of East of Olkaria Domes*. KenGen, Kenya, internal report.

Kenya Power Company, 1984: *Background report for scientific and technical review meeting.* Kenya Power Co., Ltd., internal report prepared by KRTA, 254 pp.

Lagat, J.K., 2004: *Geology, hydrothermal alteration and fluid inclusion studies of the Olkaria Domes geothermal field, Kenya.* University of Iceland, MSc thesis, UNU-GTP, Iceland, report 2, 79 pp.

Malimo, S.J., 2009: Interpretation of geochemical well test data for wells OW-903b, OW-904b and OW-909, Olkaria Domes, Kenya. Report 17 in: *Geothermal training in Iceland 2009*. UNU-GTP, Reykjavík, 319-344.

Mannvit/ÍSOR/Vatnaskil/Verkís Consortium, 2011: *Revision of the conceptual model of the Greater Olkaria geothermal system- Phase I*. Mannvit/ÍSOR/Vatnaskil/Verkís, Reykjavík, 100 pp.

Mannvit/ÍSOR/Vatnaskil/Verkís Consortium, 2012: *Development of the numerical model of the Greater Olkaria geothermal system - Phase I.* Mannvit/ÍSOR/Vatnaskil/Verkís, Reykjavík, 95 pp.

Mungania, J., 1999: *Summary of updates of the geology of the Olkaria Domes geothermal field.* KenGen - Kenya Electricity Generating Company, Ltd., unpubl. report.

Mwangi, D.W., 2012: Borehole geology and hydrothermal mineralisation of well OW–916, Olkaria Domes geothermal field, Naivasha, Kenya. Report 24 in: *Geothermal training in Iceland 2012*. UNU-GTP, Iceland, 541-571.

Ofwona, C.O., 2002: *A reservoir study of Olkaria East geothermal system, Kenya*. University of Iceland, MSc thesis, UNU-GTP, Iceland, report 1, 74 pp.

Omenda, P.A., 1998: The geology and structural controls of the Olkaria geothermal system, Kenya. *Geothermics, 27-1*, 55-74.

Pruess, K., Oldenburg, C., and Moridis, G., 1999: *TOUGH2, user's guide version 2.0*. Lawrence Berkeley National Laboratory, 197 pp.

Stefánsson, V., and Steingrímsson, B.S., 1980: *Geothermal logging I, an introduction to techniques and interpretation.* Orkustofnun, Reykjavík, report OS-80017/JHD-09, 117 pp.

Wanjohi, A., 2011: *Geophysics report east of Olkaria Domes (Akira) geothermal field.* KenGen, Kenya, internal report.

APPENDIX I: Temperature and pressure profiles with formation temperatures in selected Olkaria Domes wells

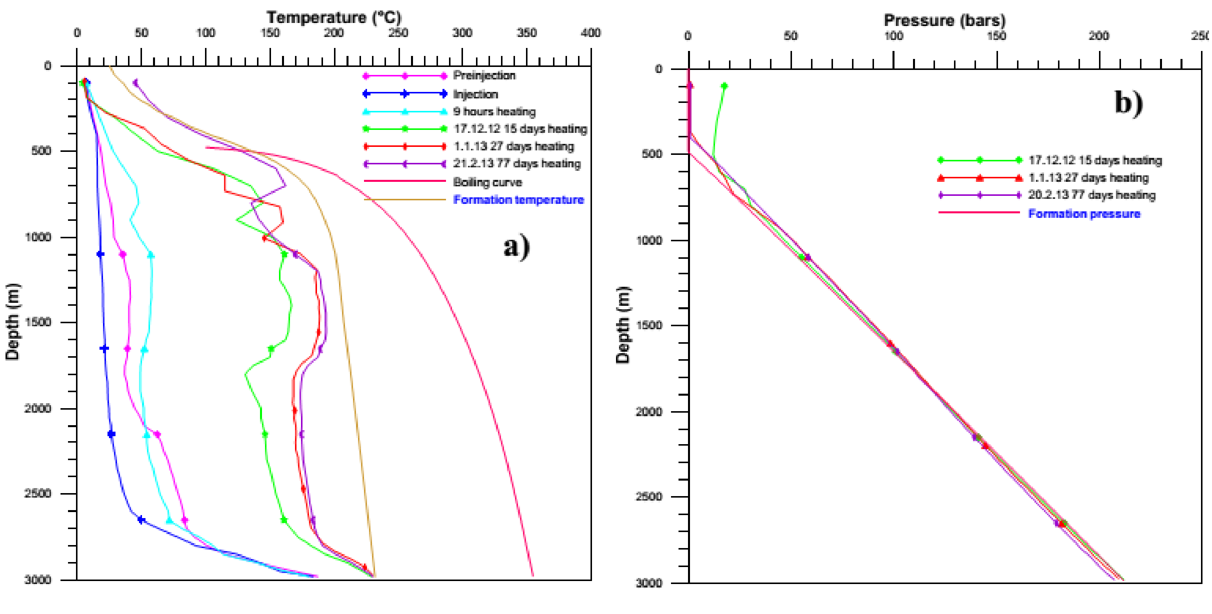

FIGURE 1: Well OW-907B: a) Temperature profiles; b) Pressure profiles

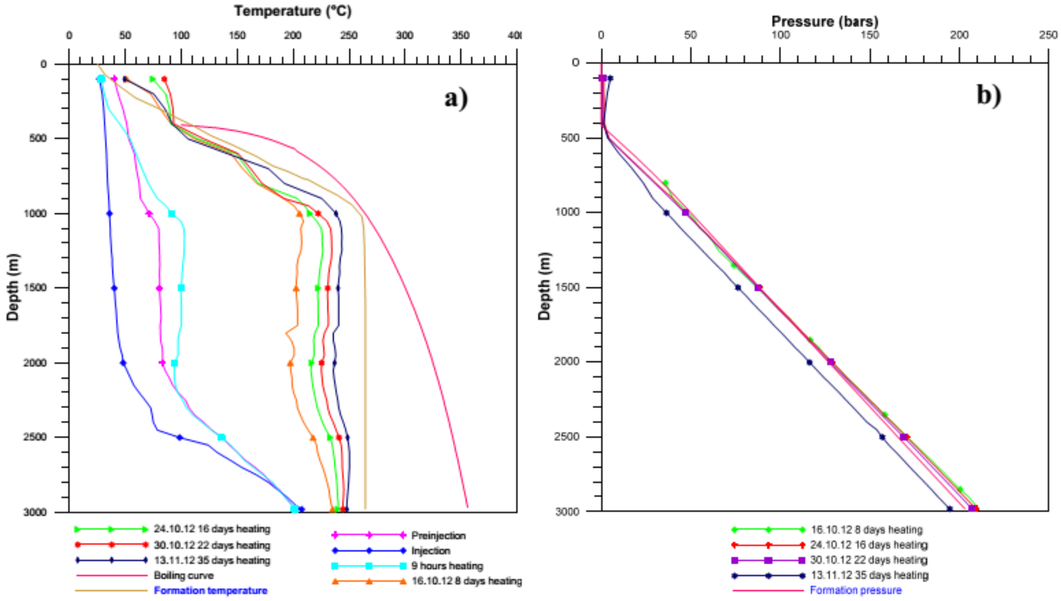

FIGURE 2: Well OW-911: a) Temperature profiles; b) Pressure profiles

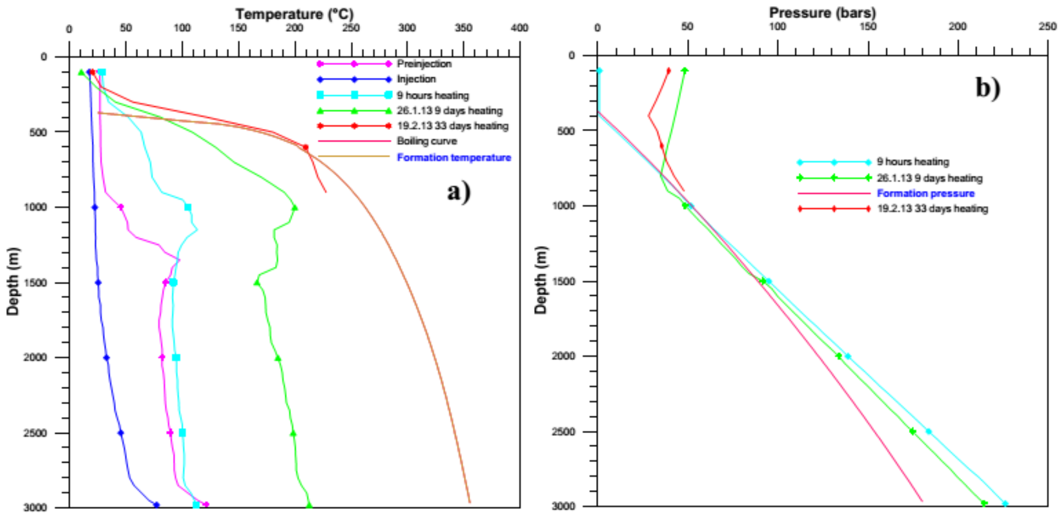

FIGURE 3: Well OW-914C: a) Temperature profiles; b) Pressure profiles

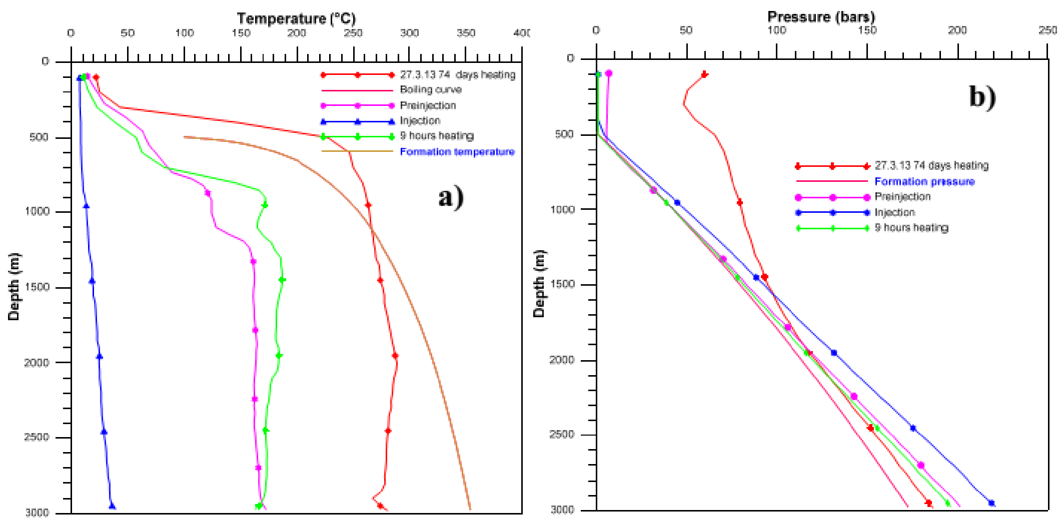

FIGURE 4: Well OW-915C: a) Temperature profiles; b) Pressure profiles

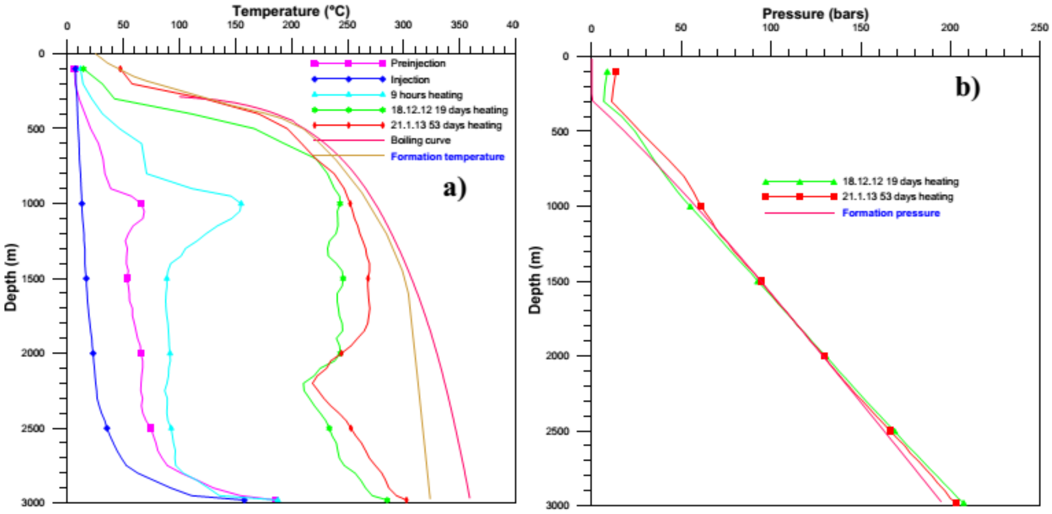

FIGURE 5: Well OW-916B: a) Temperature profiles; b) Pressure profiles

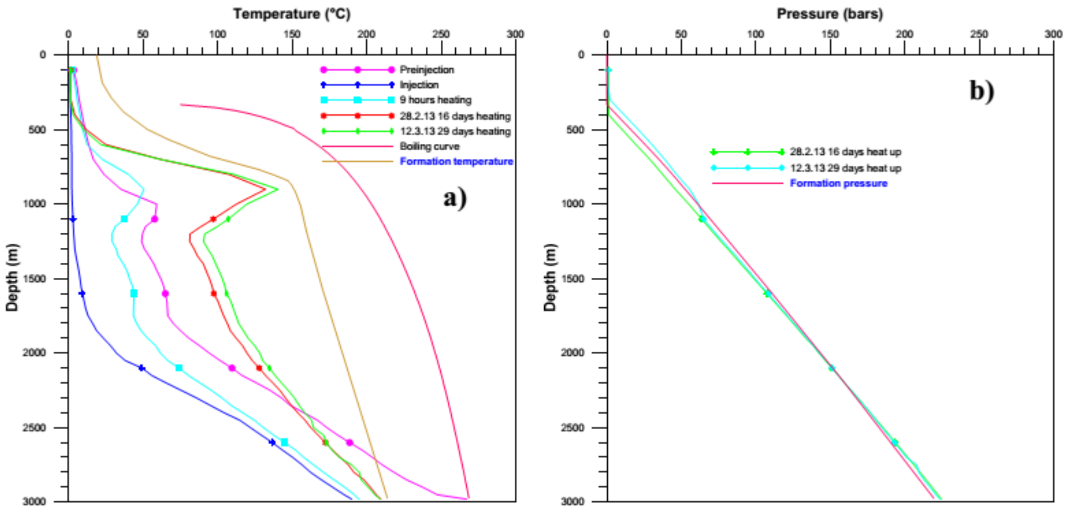

FIGURE 6: Well OW-919: a) Temperature profiles; b) Pressure profiles

APPENDIX II: Calibration results from the updated 3-D natural-state model

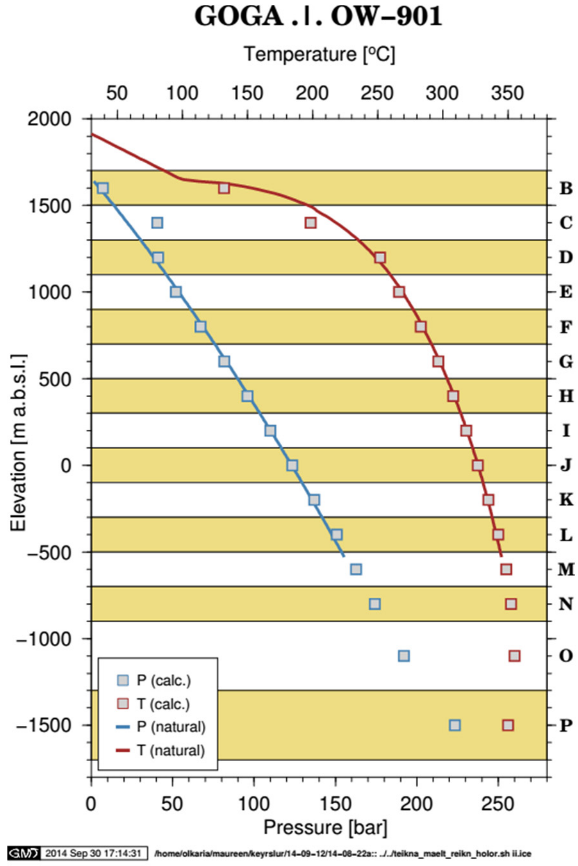

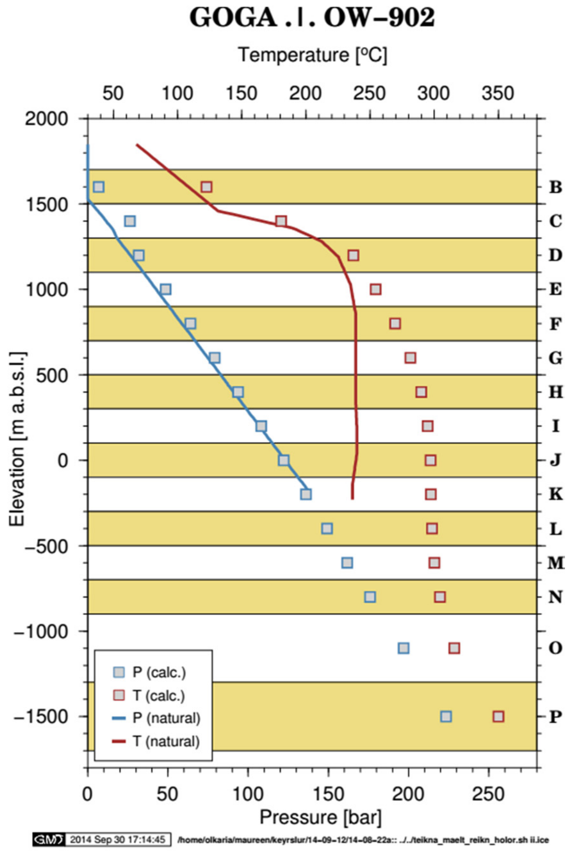

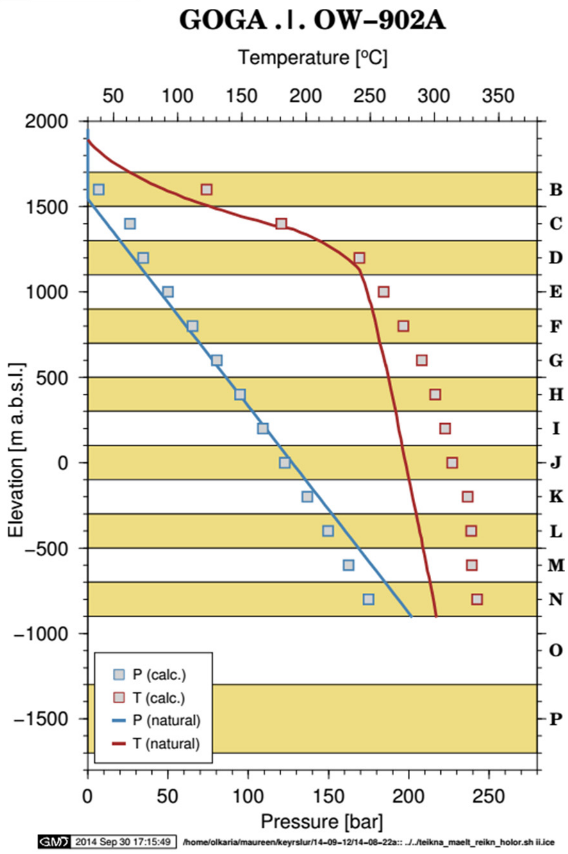

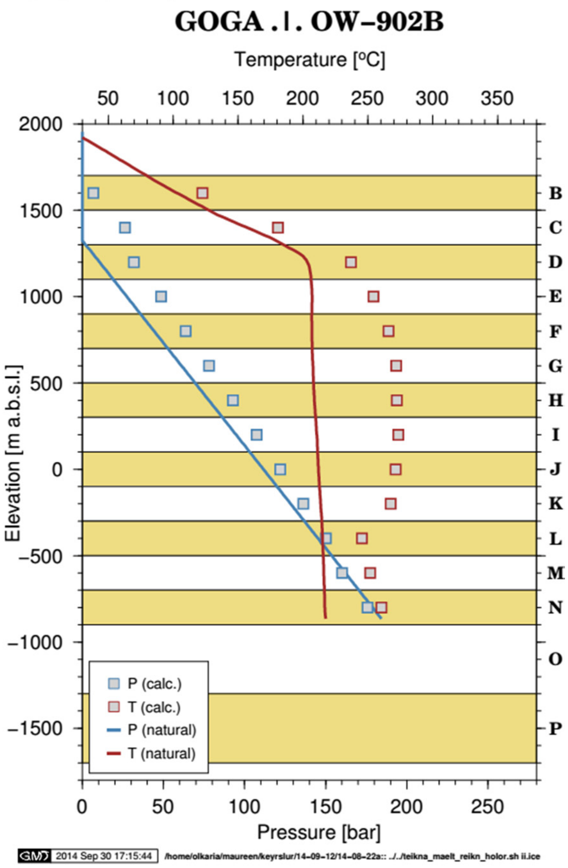

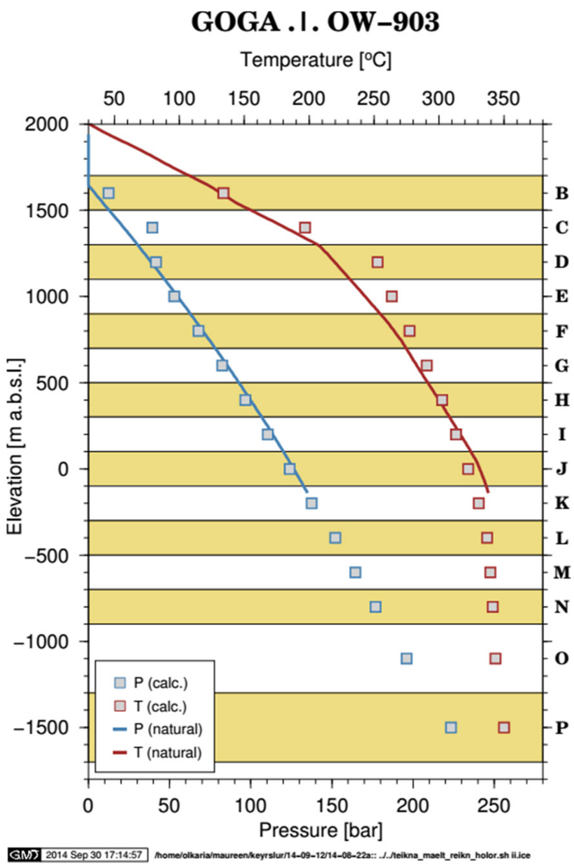
GOGA .I. OW-903
Temperature [°C]
Elevation [m a.b.s.l.]
Pressure [bar]
P (calc.)
T (calc.)
P (natural)
T (natural)
B
C
D
E
F
G
H
I
J
K
L
M
N
O
P

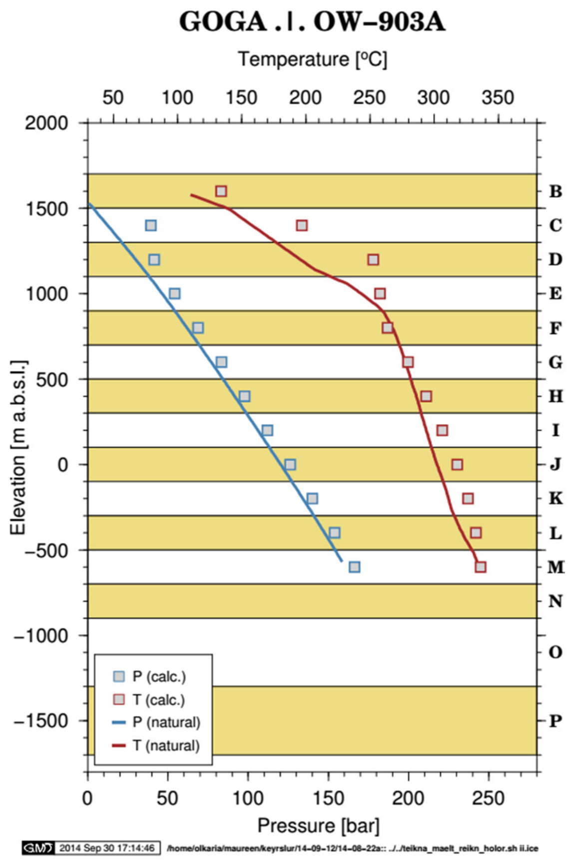
GOGA .I. OW-903A
Temperature [°C]
Elevation [m a.b.s.l.]
Pressure [bar]
P (calc.)
T (calc.)
P (natural)
T (natural)
B
C
D
E
F
G
H
I
J
K
L
M
N
O
P

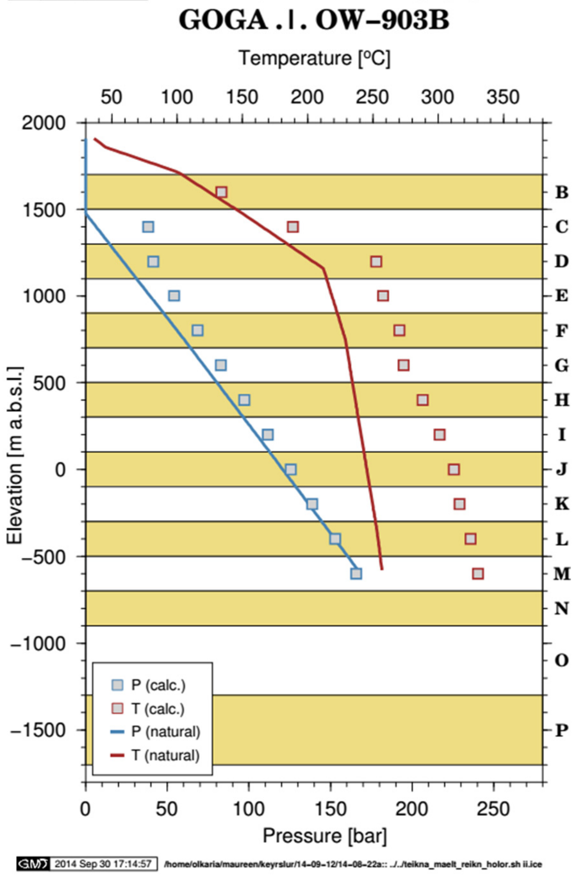
GOGA .I. OW-903B
Temperature [°C]
Elevation [m a.b.s.l.]
Pressure [bar]
P (calc.)
T (calc.)
P (natural)
T (natural)
B
C
D
E
F
G
H
I
J
K
L
M
N
O
P

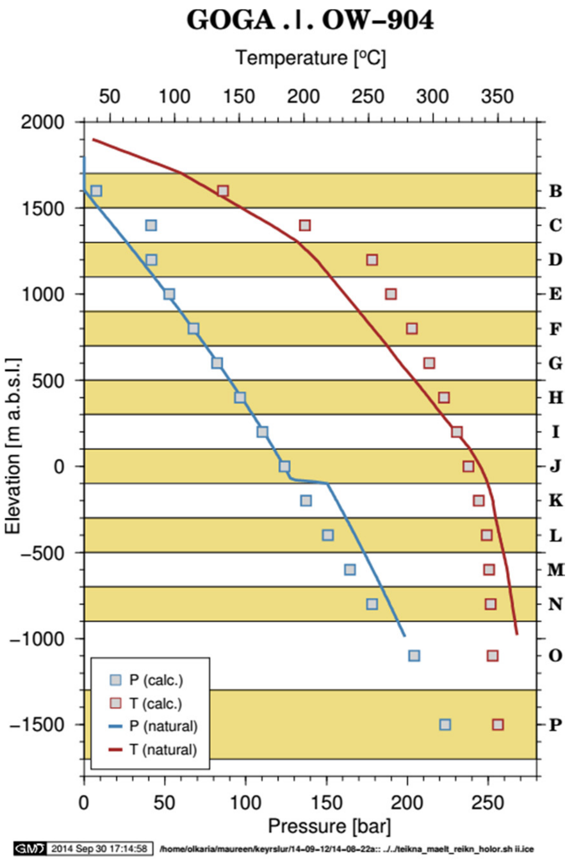
GOGA .I. OW-904
Temperature [°C]
Elevation [m a.b.s.l.]
Pressure [bar]
P (calc.)
T (calc.)
P (natural)
T (natural)
B
C
D
E
F
G
H
I
J
K
L
M
N
O
P

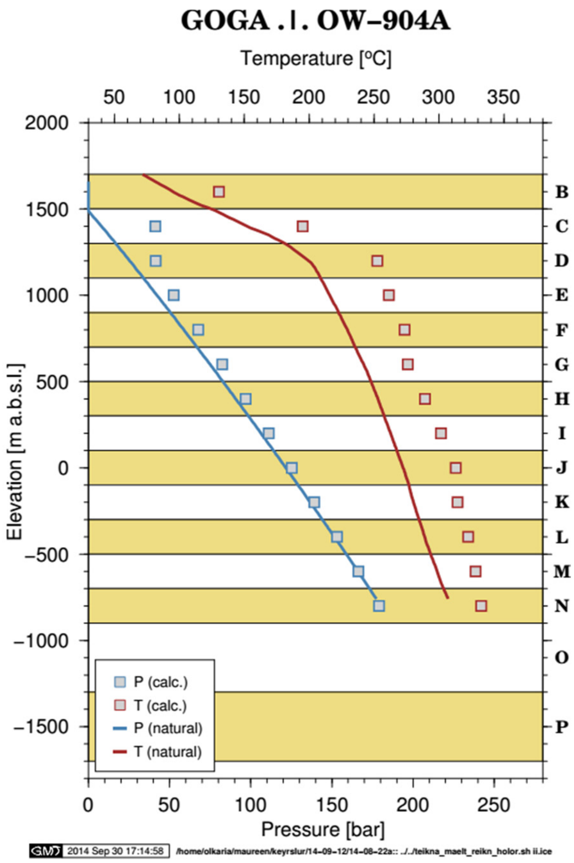
GOGA .I. OW-904A
Temperature [ºC]
Elevation [m a.b.s.l.]
Pressure [bar]
P (calc.)
T (calc.)
P (natural)
T (natural)
B
C
D
E
F
G
H
I
J
K
L
M
N
O
P

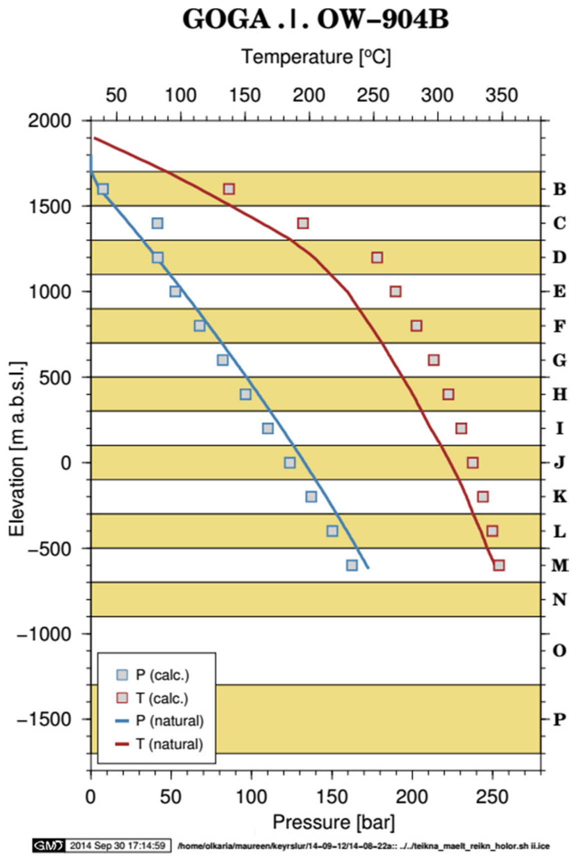
GOGA .I. OW-904B
Temperature [ºC]
Elevation [m a.b.s.l.]
Pressure [bar]
P (calc.)
T (calc.)
P (natural)
T (natural)
B
C
D
E
F
G
H
I
J
K
L
M
N
O
P

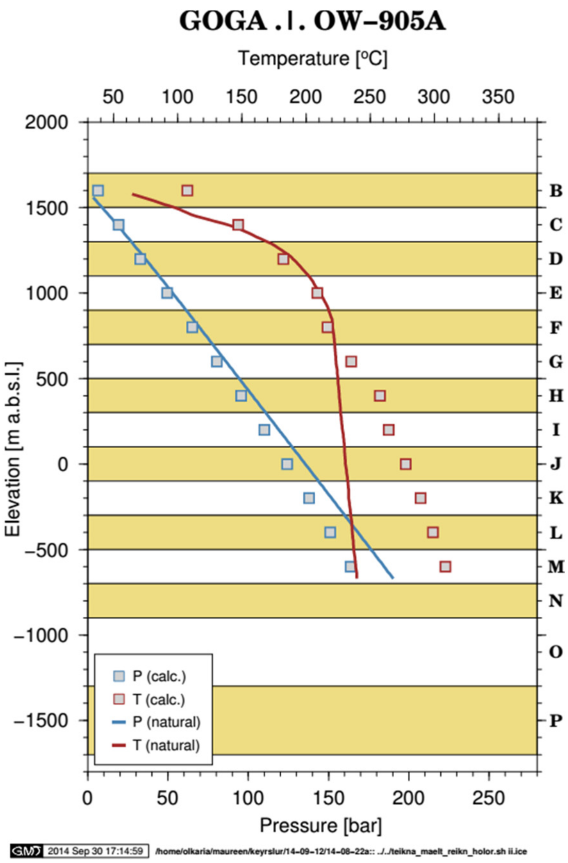
GOGA .I. OW-905A
Temperature [ºC]
Elevation [m a.b.s.l.]
Pressure [bar]
P (calc.)
T (calc.)
P (natural)
T (natural)
B
C
D
E
F
G
H
I
J
K
L
M
N
O
P

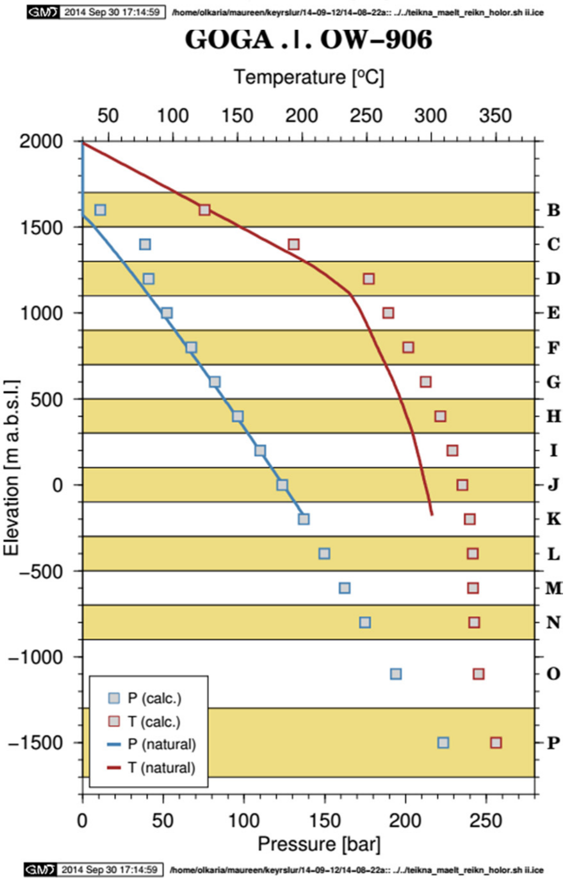
GOGA .I. OW-906
Temperature [ºC]
Elevation [m a.b.s.l.]
Pressure [bar]
P (calc.)
T (calc.)
P (natural)
T (natural)
B
C
D
E
F
G
H
I
J
K
L
M
N
O
P

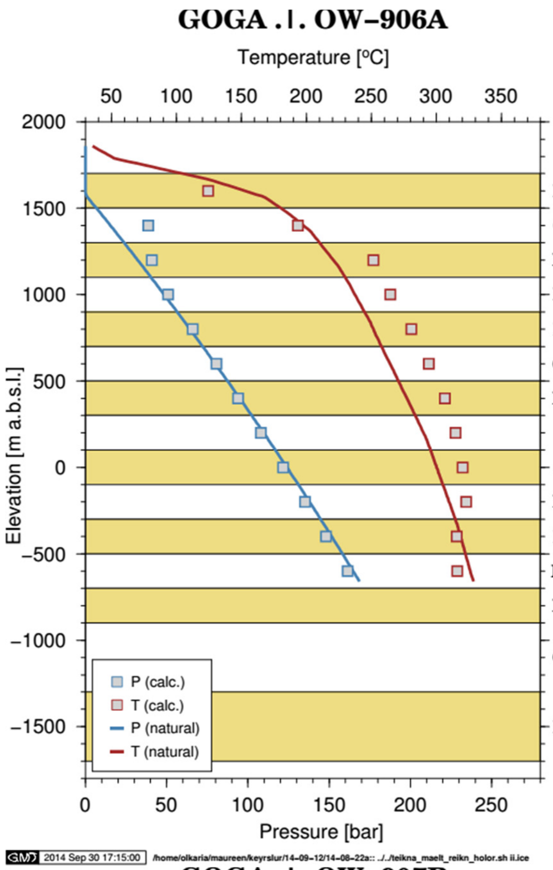
GOGA .I. OW-906A
Temperature [°C]
Elevation [m a.b.s.l.]
Pressure [bar]
P (calc.)
T (calc.)
P (natural)
T (natural)
B C D E F G H I J K L M N O P

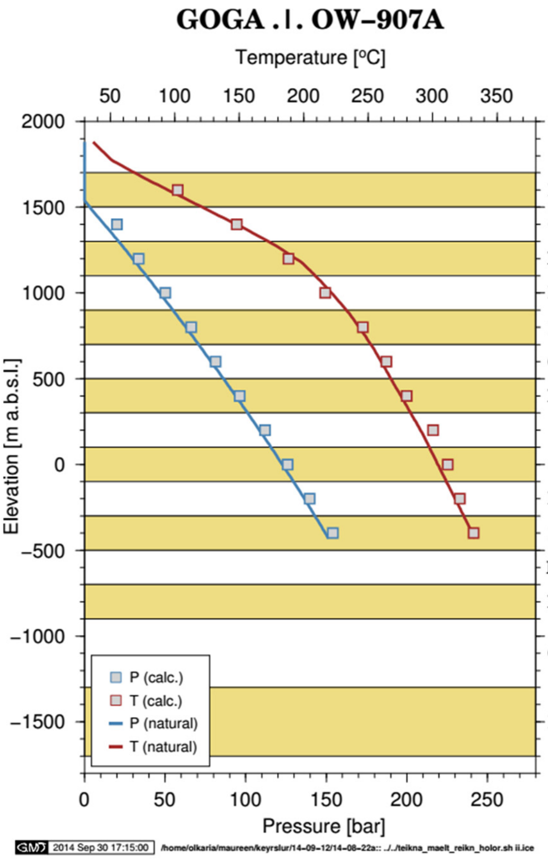
GOGA .I. OW-907A
Temperature [°C]
Elevation [m a.b.s.l.]
Pressure [bar]
P (calc.)
T (calc.)
P (natural)
T (natural)
B C D E F G H I J K L M N O P

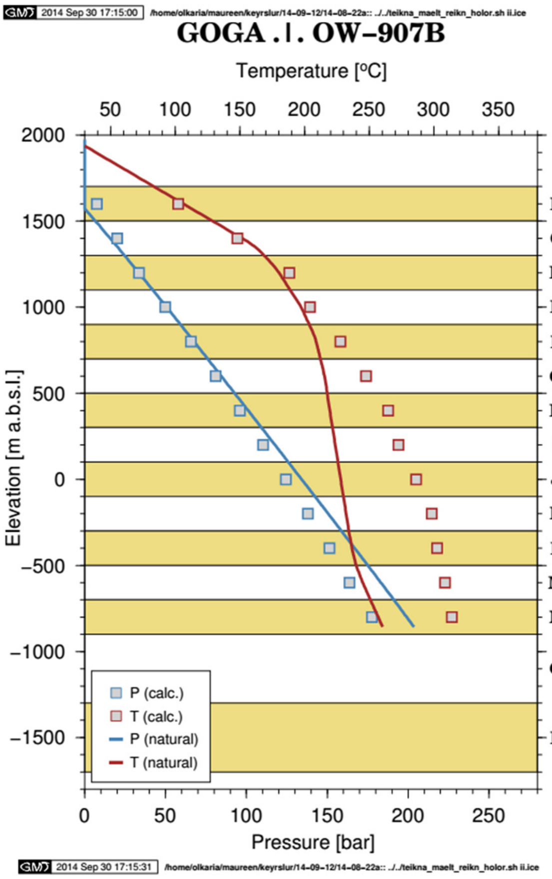
GOGA .I. OW-907B
Temperature [°C]
Elevation [m a.b.s.l.]
Pressure [bar]
P (calc.)
T (calc.)
P (natural)
T (natural)
B C D E F G H I J K L M N O P

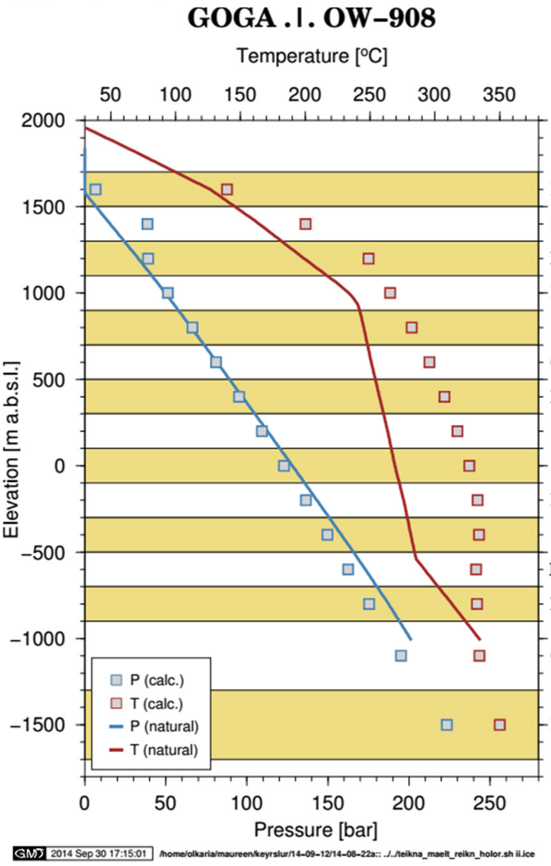
GOGA .I. OW-908
Temperature [°C]
Elevation [m a.b.s.l.]
Pressure [bar]
P (calc.)
T (calc.)
P (natural)
T (natural)
B C D E F G H I J K L M N O P

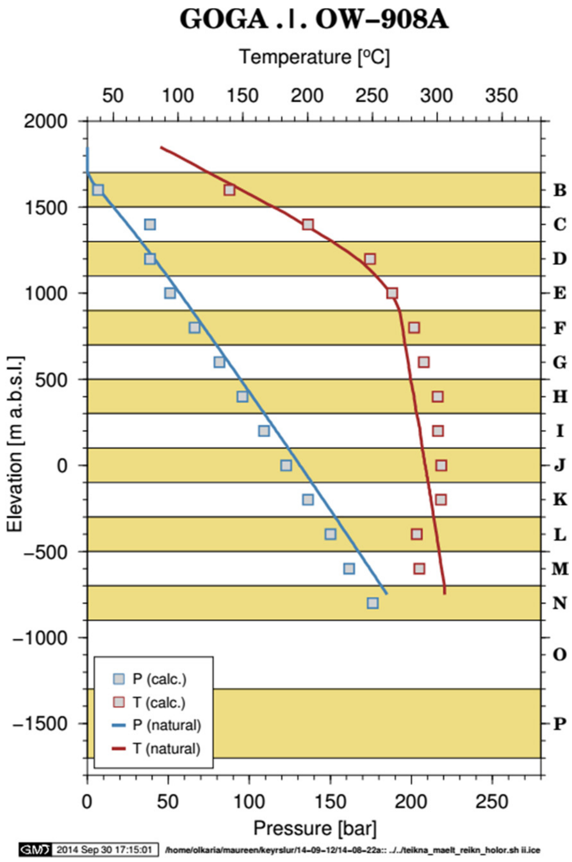
GOGA .I. OW-908A
Temperature [°C]
Elevation [m a.b.s.l.]
Pressure [bar]
B
C
D
E
F
G
H
I
J
K
L
M
N
O
P
P (calc.)
T (calc.)
P (natural)
T (natural)

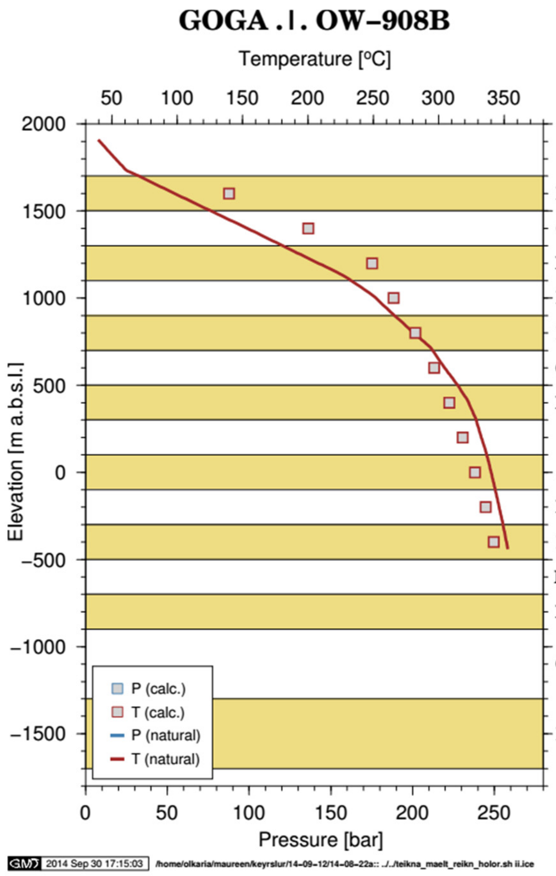
GOGA .I. OW-908B
Temperature [°C]
Elevation [m a.b.s.l.]
Pressure [bar]
B
C
D
E
F
G
H
I
J
K
L
M
N
O
P
P (calc.)
T (calc.)
P (natural)
T (natural)

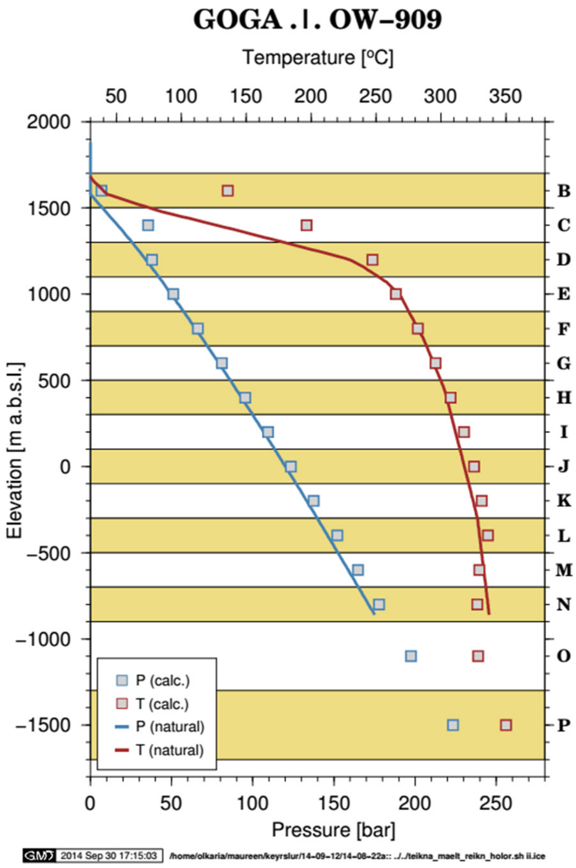
GOGA .I. OW-909
Temperature [°C]
Elevation [m a.b.s.l.]
Pressure [bar]
B
C
D
E
F
G
H
I
J
K
L
M
N
O
P
P (calc.)
T (calc.)
P (natural)
T (natural)

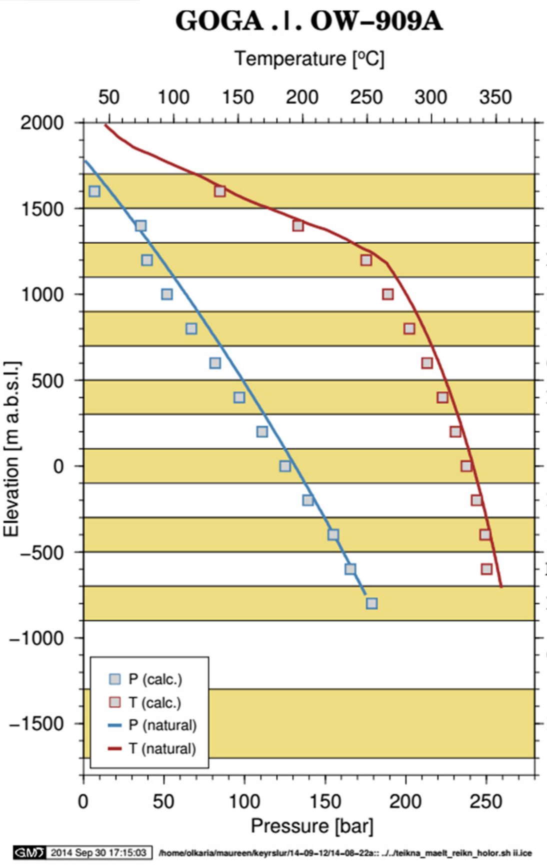
GOGA .I. OW-909A
Temperature [°C]
Elevation [m a.b.s.l.]
Pressure [bar]
B
C
D
E
F
G
H
I
J
K
L
M
N
O
P
P (calc.)
T (calc.)
P (natural)
T (natural)

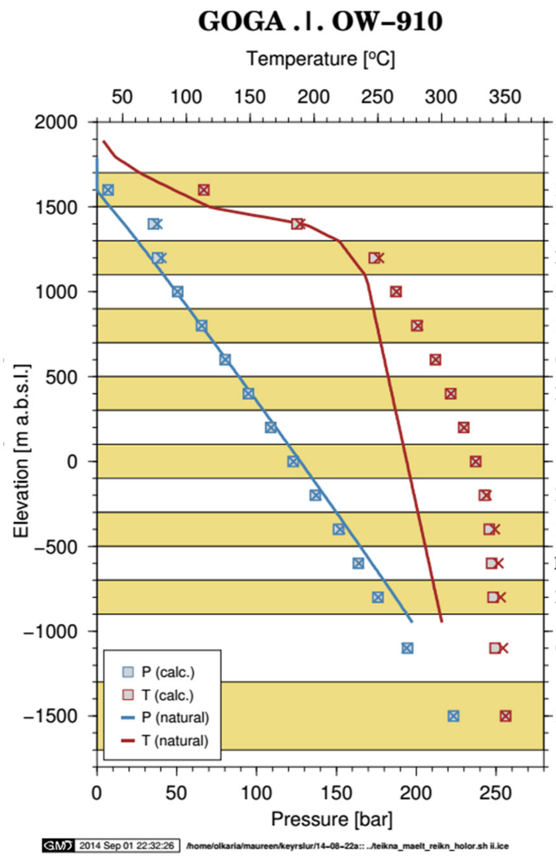
GOGA .I. OW-910
Temperature [ºC]
Elevation [m a.s.l.]
Pressure [bar]
P (calc.)
T (calc.)
P (natural)
T (natural)
B
C
D
E
F
G
H
I
J
K
L
M
N
O
P
2014 Sep 01 22:32:26

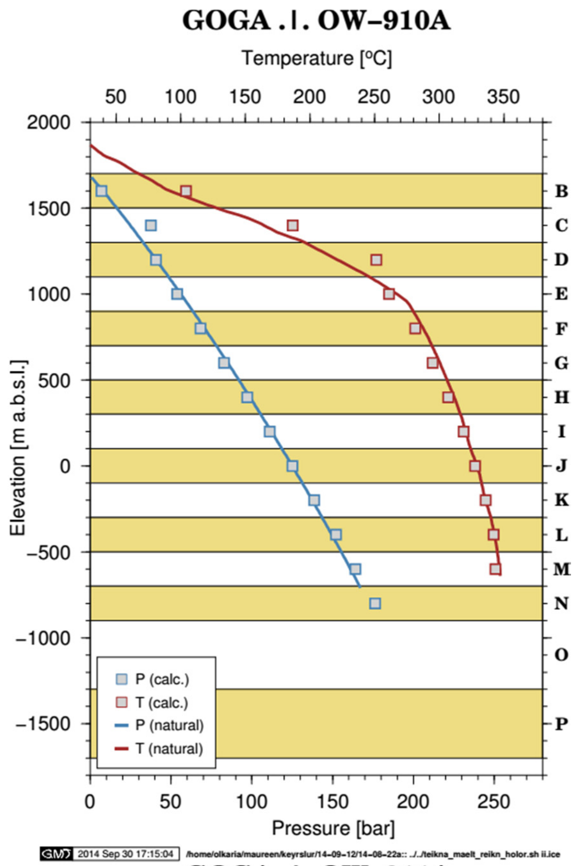
GOGA .I. OW-910A
Temperature [ºC]
Elevation [m a.s.l.]
Pressure [bar]
P (calc.)
T (calc.)
P (natural)
T (natural)
B
C
D
E
F
G
H
I
J
K
L
M
N
O
P
2014 Sep 30 17:15:04

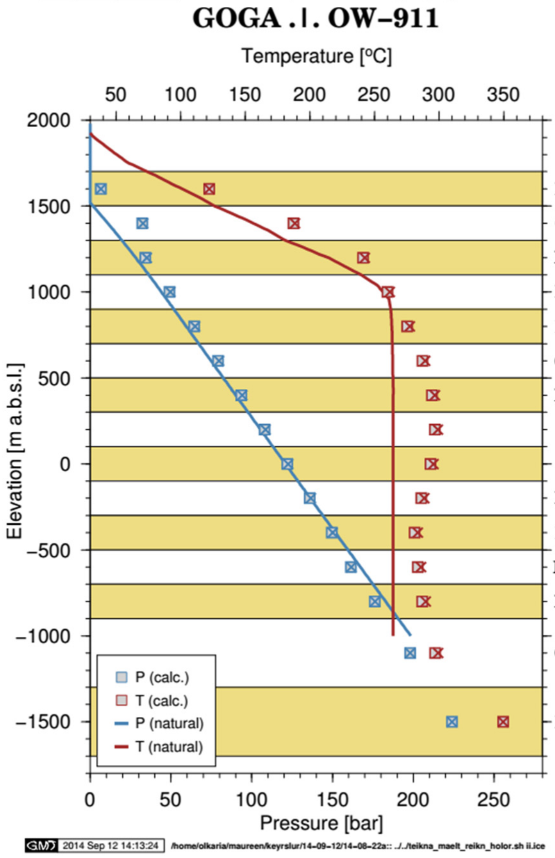
GOGA .I. OW-911
Temperature [ºC]
Elevation [m a.s.l.]
Pressure [bar]
P (calc.)
T (calc.)
P (natural)
T (natural)
B
C
D
E
F
G
H
I
J
K
L
M
N
O
P
2014 Sep 12 14:13:24

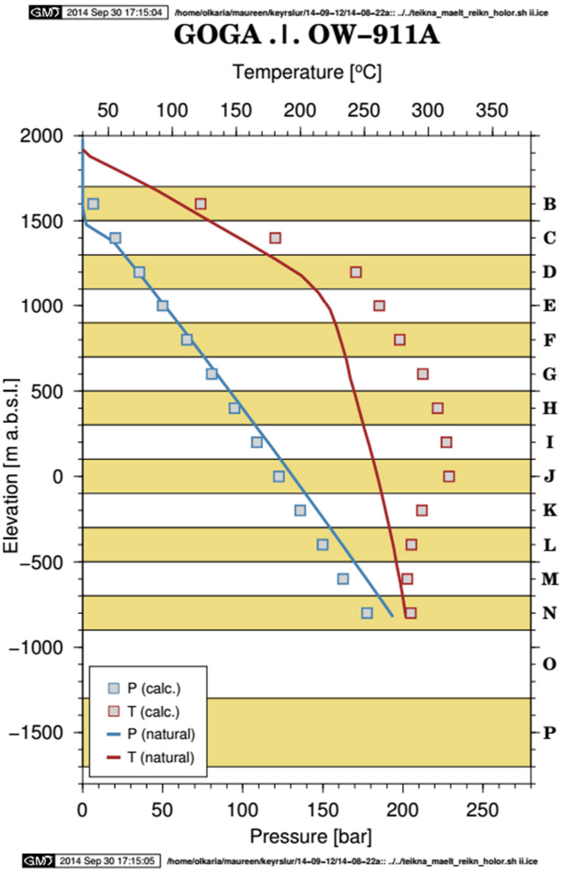
GOGA .I. OW-911A
Temperature [ºC]
Elevation [m a.s.l.]
Pressure [bar]
P (calc.)
T (calc.)
P (natural)
T (natural)
B
C
D
E
F
G
H
I
J
K
L
M
N
O
P
2014 Sep 30 17:15:05

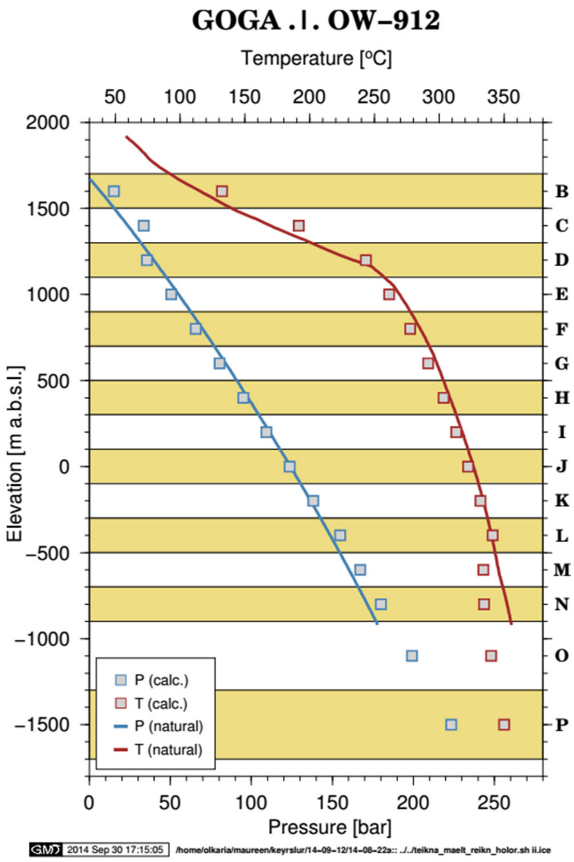
GOGA .I. OW-912
Temperature [°C]
Elevation [m a.s.l.]
Pressure [bar]
B
C
D
E
F
G
H
I
J
K
L
M
N
O
P
P (calc.)
T (calc.)
P (natural)
T (natural)

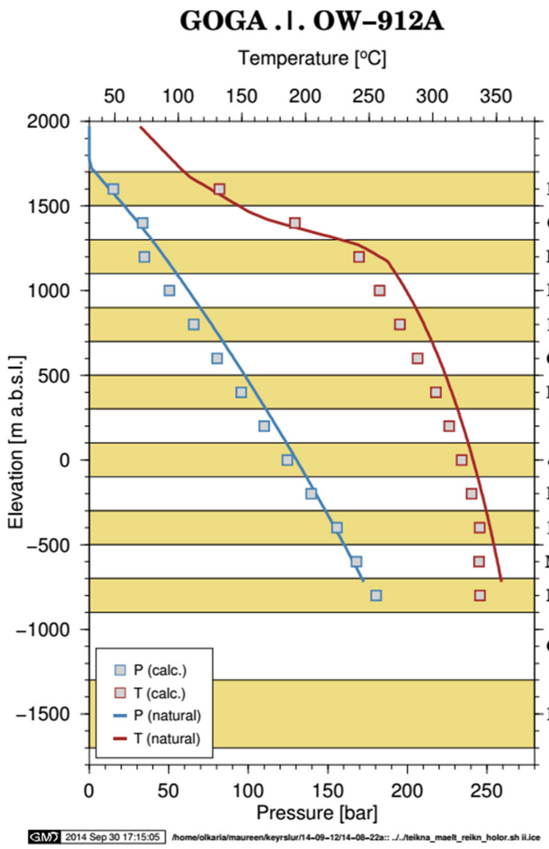
GOGA .I. OW-912A
Temperature [°C]
Elevation [m a.s.l.]
Pressure [bar]
B
C
D
E
F
G
H
I
J
K
L
M
N
O
P
P (calc.)
T (calc.)
P (natural)
T (natural)

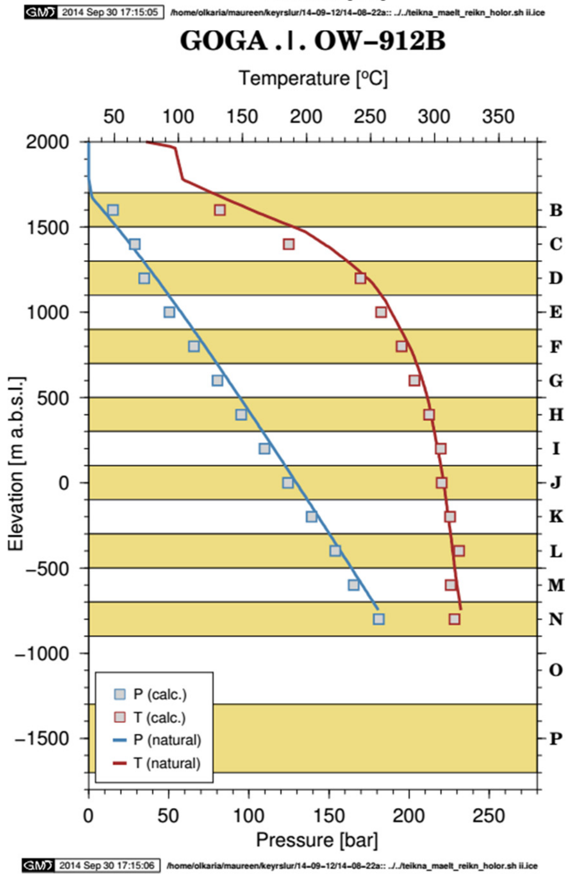
GOGA .I. OW-912B
Temperature [°C]
Elevation [m a.s.l.]
Pressure [bar]
B
C
D
E
F
G
H
I
J
K
L
M
N
O
P
P (calc.)
T (calc.)
P (natural)
T (natural)

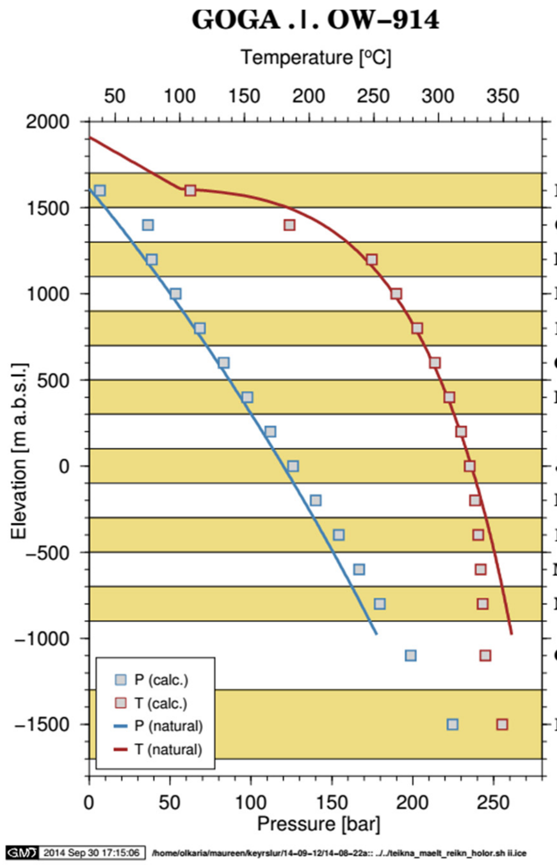
GOGA .I. OW-914
Temperature [°C]
Elevation [m a.s.l.]
Pressure [bar]
B
C
D
E
F
G
H
I
J
K
L
M
N
O
P
P (calc.)
T (calc.)
P (natural)
T (natural)

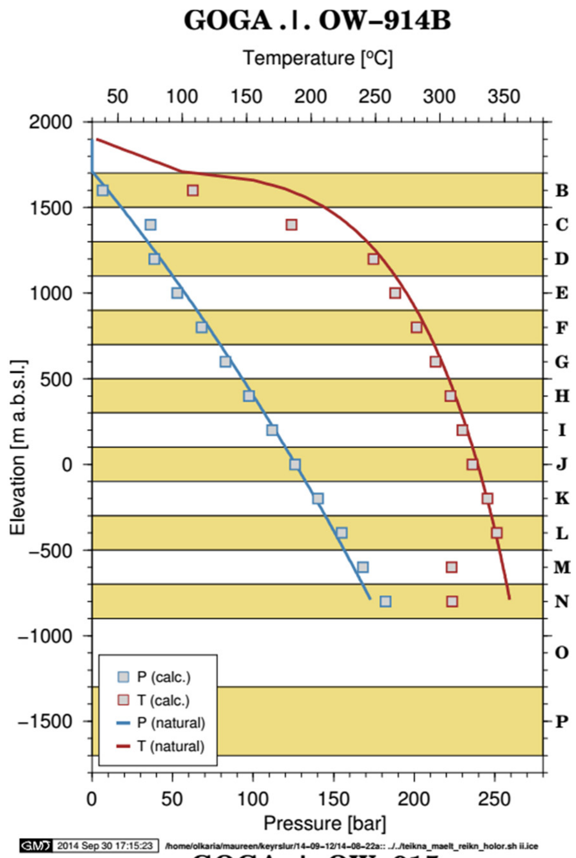
GOGA .I. OW-914B
Temperature [°C]
50 100 150 200 250 300 350
Elevation [m a.b.s.l.]
2000 1500 1000 500 0 -500 -1000 -1500
B C D E F G H I J K L M N O P
P (calc.)
T (calc.)
P (natural)
T (natural)
0 50 100 150 200 250
Pressure [bar]

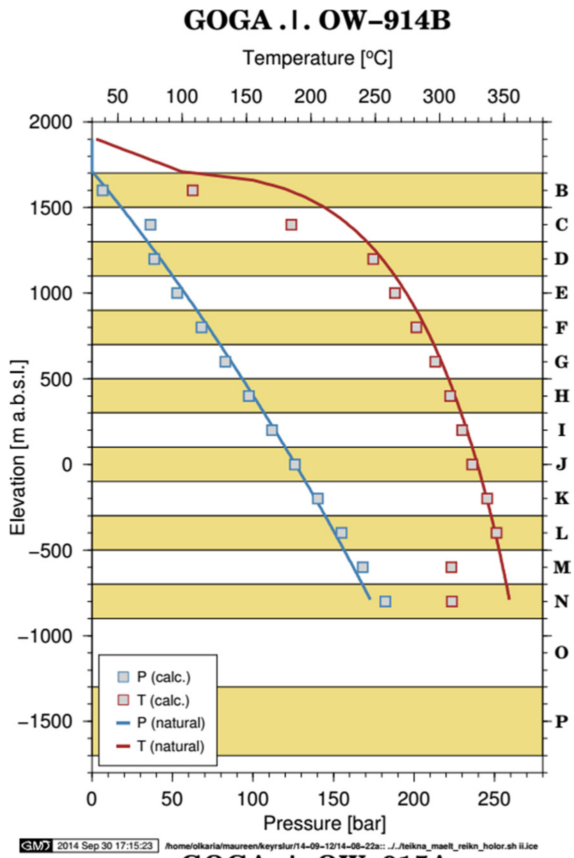
GOGA .I. OW-914B
Temperature [°C]
50 100 150 200 250 300 350
Elevation [m a.b.s.l.]
2000 1500 1000 500 0 -500 -1000 -1500
B C D E F G H I J K L M N O P
P (calc.)
T (calc.)
P (natural)
T (natural)
0 50 100 150 200 250
Pressure [bar]

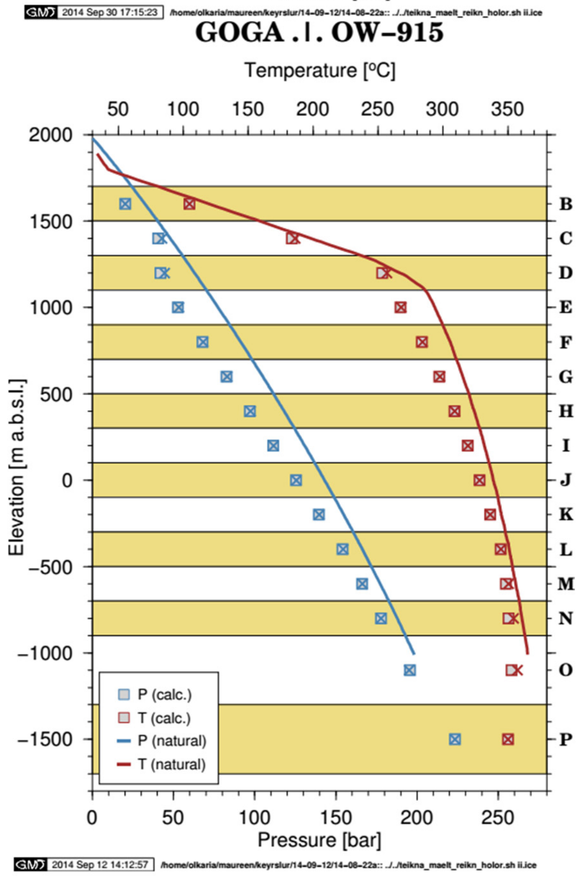
GOGA .I. OW-915
Temperature [°C]
50 100 150 200 250 300 350
Elevation [m a.b.s.l.]
2000 1500 1000 500 0 -500 -1000 -1500
B C D E F G H I J K L M N O P
P (calc.)
T (calc.)
P (natural)
T (natural)
0 50 100 150 200 250
Pressure [bar]

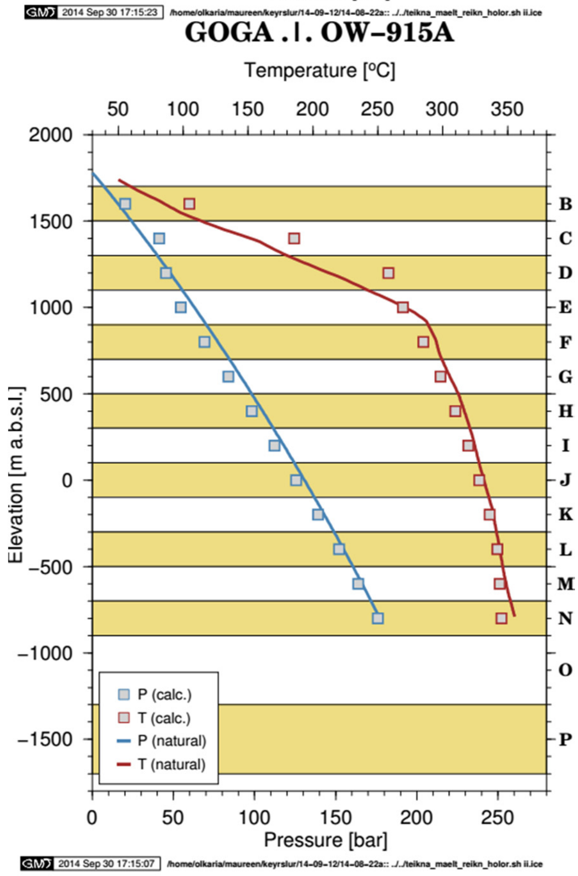
GOGA .I. OW-915A
Temperature [°C]
50 100 150 200 250 300 350
Elevation [m a.b.s.l.]
2000 1500 1000 500 0 -500 -1000 -1500
B C D E F G H I J K L M N O P
P (calc.)
T (calc.)
P (natural)
T (natural)
0 50 100 150 200 250
Pressure [bar]

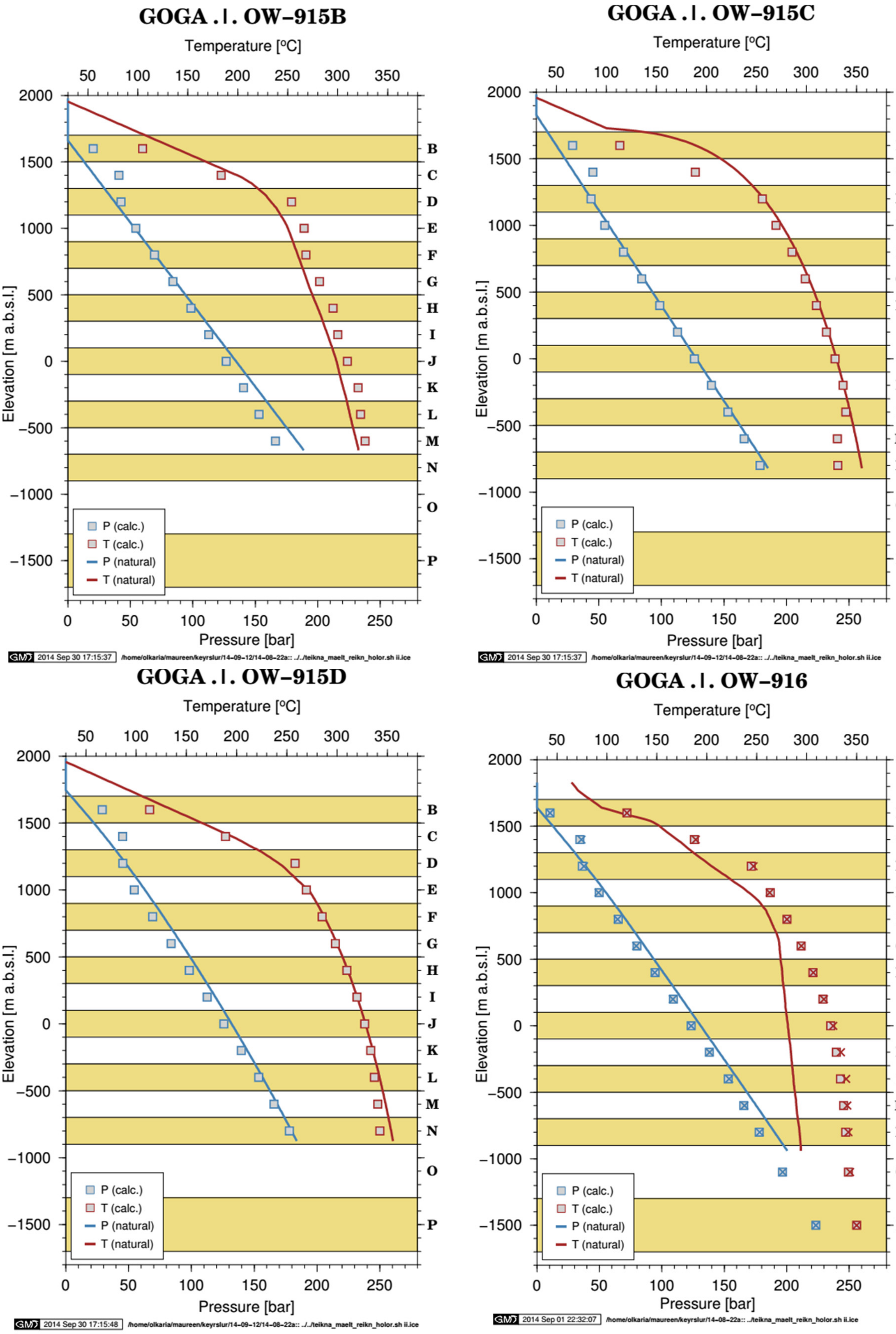
GOGA .l. OW-915B
Temperature [°C]
Elevation [m a.b.s.l.]
Pressure [bar]
P (calc.)
T (calc.)
P (natural)
T (natural)
B C D E F G H I J K L M N O P
GOGA .l. OW-915C
Temperature [°C]
Elevation [m a.b.s.l.]
Pressure [bar]
P (calc.)
T (calc.)
P (natural)
T (natural)
GOGA .l. OW-915D
Temperature [°C]
Elevation [m a.b.s.l.]
Pressure [bar]
P (calc.)
T (calc.)
P (natural)
T (natural)
GOGA .l. OW-916
Temperature [°C]
Elevation [m a.b.s.l.]
Pressure [bar]
P (calc.)
T (calc.)
P (natural)
T (natural)

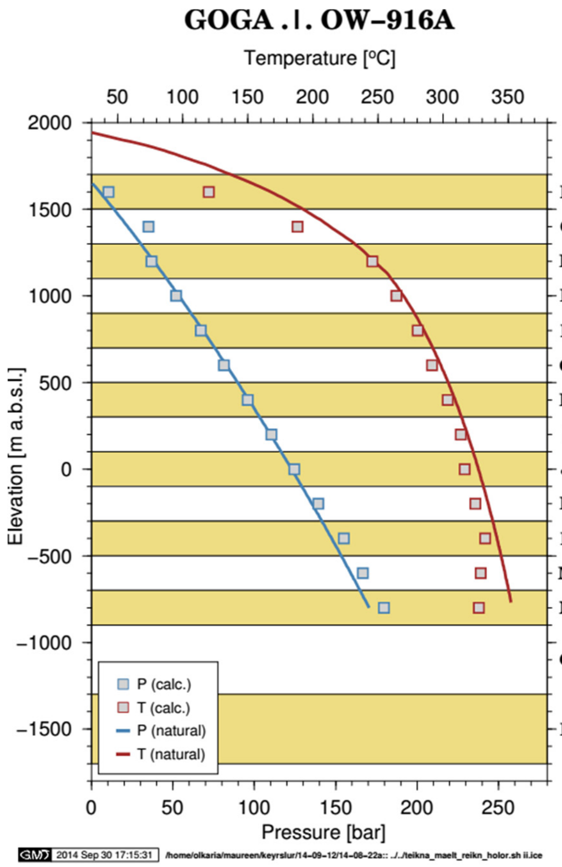
GOGA .l. OW-916A
Temperature [°C]
50 100 150 200 250 300 350
2000 1500 1000 500 0 −500 −1000 −1500
Elevation [m a.b.s.l.]
B C D E F G H I J K L M N O P
P (calc.)
T (calc.)
P (natural)
T (natural)
0 50 100 150 200 250
Pressure [bar]
GMT 2014 Sep 30 17:15:31
/home/olkaria/maureen/keyrslur/14-09-12/14-08-22a:: ../../teikna_maelt_reikn_holor.sh ii.ice

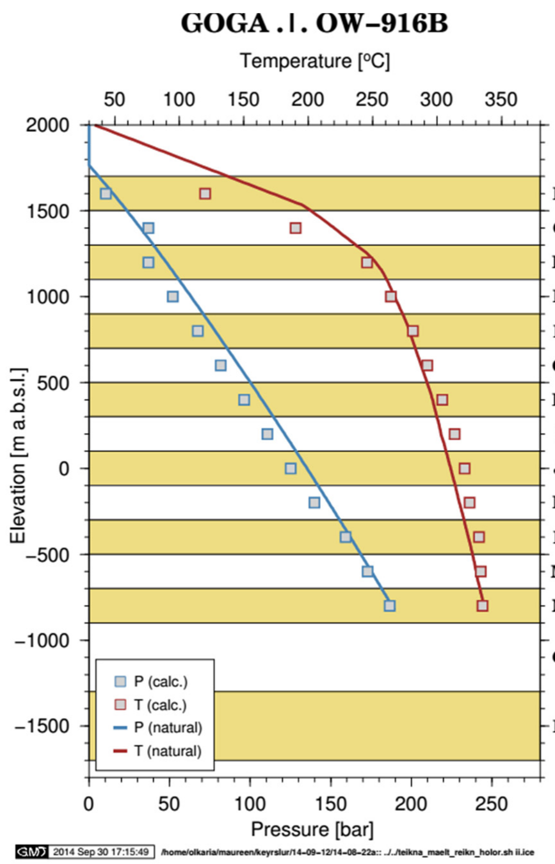
GOGA .l. OW-916B
Temperature [°C]
50 100 150 200 250 300 350
2000 1500 1000 500 0 −500 −1000 −1500
Elevation [m a.b.s.l.]
B C D E F G H I J K L M N O P
P (calc.)
T (calc.)
P (natural)
T (natural)
0 50 100 150 200 250
Pressure [bar]
GMT 2014 Sep 30 17:15:49
/home/olkaria/maureen/keyrslur/14-09-12/14-08-22a:: ../../teikna_maelt_reikn_holor.sh ii.ice

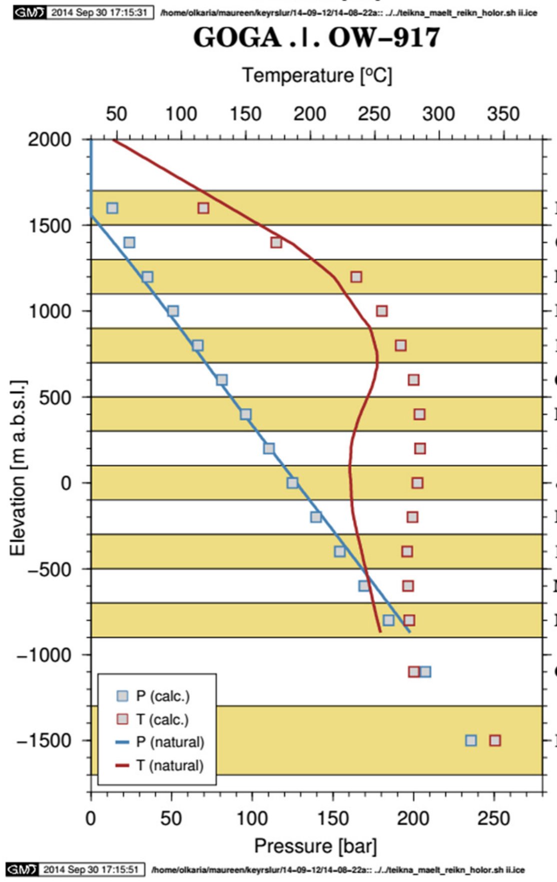
GOGA .l. OW-917
Temperature [°C]
50 100 150 200 250 300 350
2000 1500 1000 500 0 −500 −1000 −1500
Elevation [m a.b.s.l.]
B C D E F G H I J K L M N O P
P (calc.)
T (calc.)
P (natural)
T (natural)
0 50 100 150 200 250
Pressure [bar]
GMT 2014 Sep 30 17:15:51
/home/olkaria/maureen/keyrslur/14-09-12/14-08-22a:: ../../teikna_maelt_reikn_holor.sh ii.ice

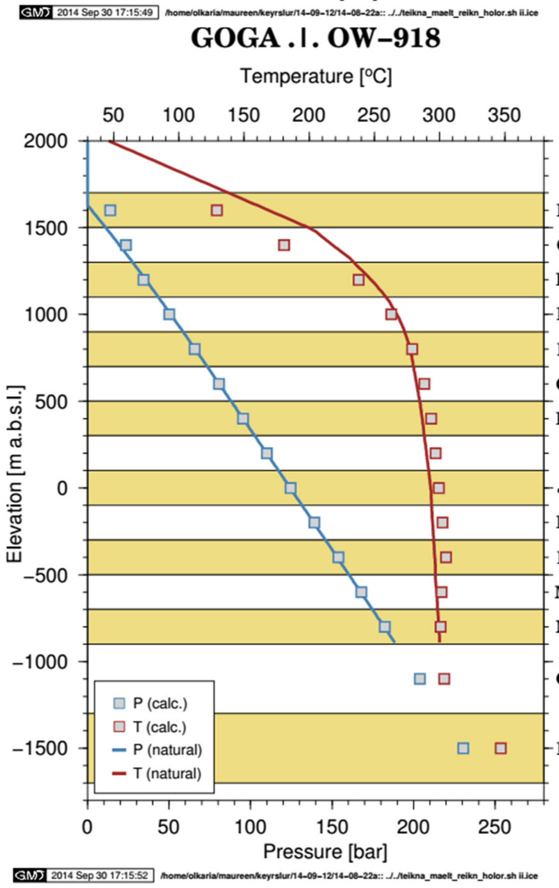
GOGA .l. OW-918
Temperature [°C]
50 100 150 200 250 300 350
2000 1500 1000 500 0 −500 −1000 −1500
Elevation [m a.b.s.l.]
B C D E F G H I J K L M N O P
P (calc.)
T (calc.)
P (natural)
T (natural)
0 50 100 150 200 250
Pressure [bar]
GMT 2014 Sep 30 17:15:52
/home/olkaria/maureen/keyrslur/14-09-12/14-08-22a:: ../../teikna_maelt_reikn_holor.sh ii.ice

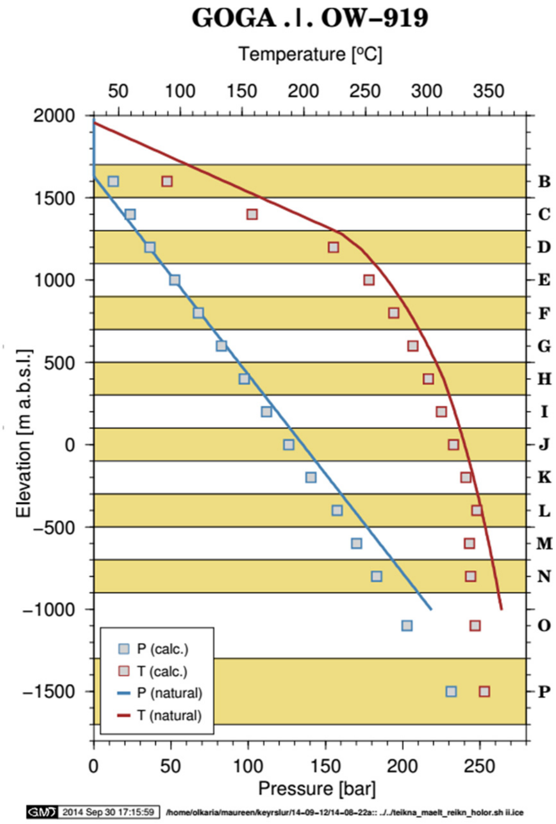
GOGA .I. OW-919
Temperature [ºC]
50 100 150 200 250 300 350
Elevation [m a.b.s.l.]
2000 1500 1000 500 0 −500 −1000 −1500
B C D E F G H I J K L M N O P
P (calc.)
T (calc.)
P (natural)
T (natural)
0 50 100 150 200 250
Pressure [bar]

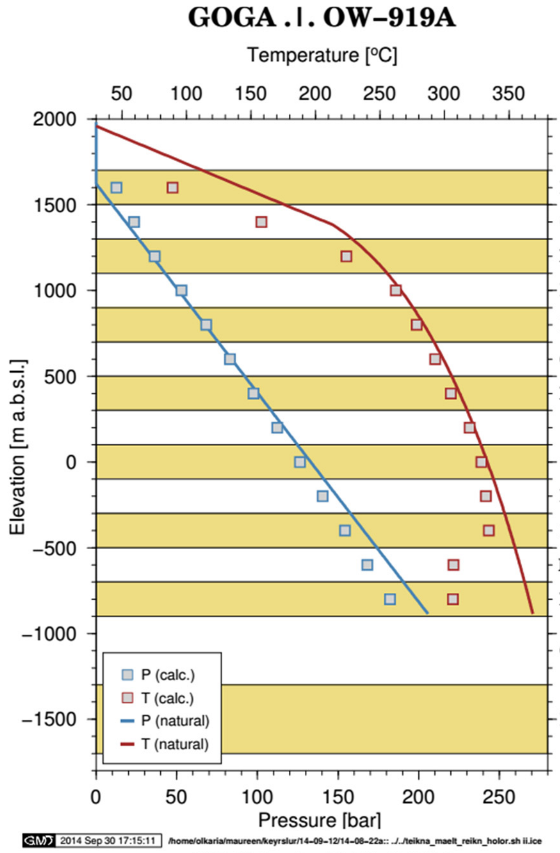
GOGA .I. OW-919A
Temperature [ºC]
50 100 150 200 250 300 350
Elevation [m a.b.s.l.]
2000 1500 1000 500 0 −500 −1000 −1500
B C D E F G H I J K L M N O P
P (calc.)
T (calc.)
P (natural)
T (natural)
0 50 100 150 200 250
Pressure [bar]

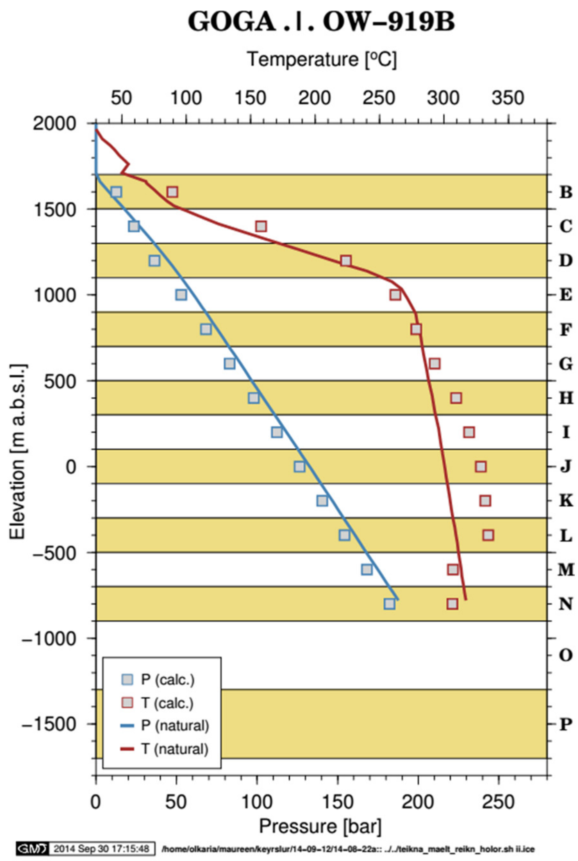
GOGA .I. OW-919B
Temperature [ºC]
50 100 150 200 250 300 350
Elevation [m a.b.s.l.]
2000 1500 1000 500 0 −500 −1000 −1500
B C D E F G H I J K L M N O P
P (calc.)
T (calc.)
P (natural)
T (natural)
0 50 100 150 200 250
Pressure [bar]

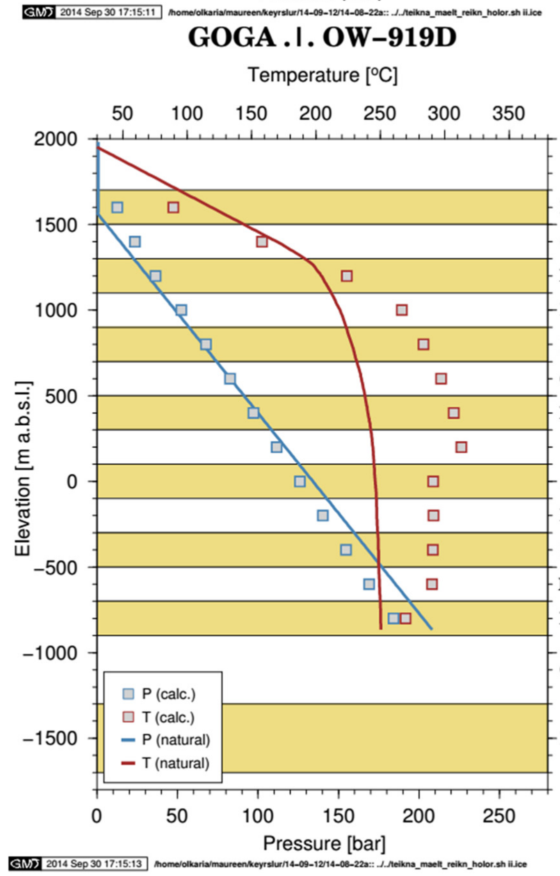
GOGA .I. OW-919D
Temperature [ºC]
50 100 150 200 250 300 350
Elevation [m a.b.s.l.]
2000 1500 1000 500 0 −500 −1000 −1500
B C D E F G H I J K L M N O P
P (calc.)
T (calc.)
P (natural)
T (natural)
0 50 100 150 200 250
Pressure [bar]

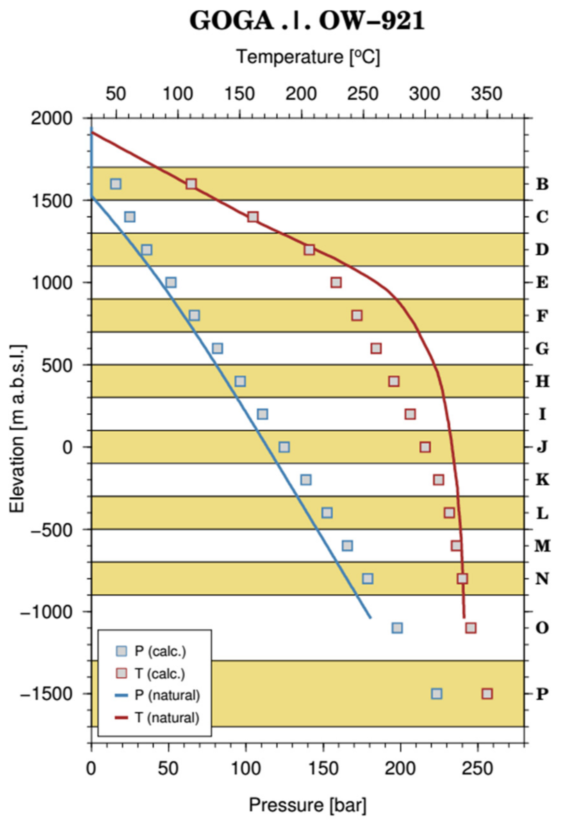
GOGA .I. OW-921
Temperature [ºC]
Elevation [m a.b.s.l.]
Pressure [bar]
P (calc.)
T (calc.)
P (natural)
T (natural)
B
C
D
E
F
G
H
I
J
K
L
M
N
O
P

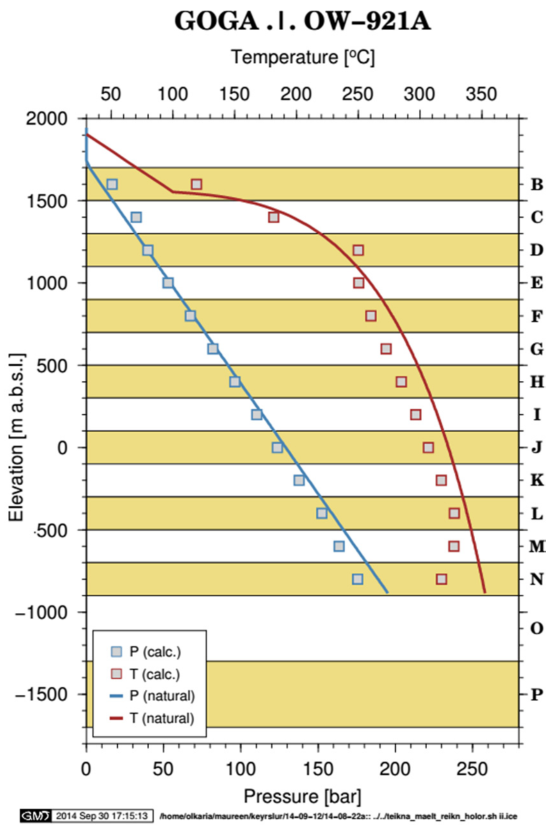
GOGA .I. OW-921A
Temperature [ºC]
Elevation [m a.b.s.l.]
Pressure [bar]
P (calc.)
T (calc.)
P (natural)
T (natural)
B
C
D
E
F
G
H
I
J
K
L
M
N
O
P
GMT 2014 Sep 30 17:15:13